運輸省港湾技術研究所

港湾技術研究所報告

REPORT OF
THE PORT AND HARBOUR RESEARCH INSTITUTE
MINISTRY OF TRANSPORT

VOL. 21 NO. 2 JUNE 1982

NAGASE, YOKOSUKA, JAPAN

港湾技術研究所報告 (REPORT OF P.H.R.I.)

第21巻 第2号 (Vol. 21, No. 2), 1982年6月 (June 1982)

目 次 (CONTENTS)

REPORT OF THE PORT AND
HARBOUR RESEARCH INSTITUTE
Vol. 21, No. 2 (June 1982)

1. Theoretical Properties of Oblique Waves Generated by Serpent-type Wavemakers

Tomotsuka TAKAYAMA*

Synopsis

Real sea waves are well known to have a property of directional randomness. Reproduction of waves with such property in laboratories is much desired for the studies of wave transformations, wave and structure interactions, and others. Though the generation of the directional random waves makes use of oblique wave system as component waves, there has been no theory which can predict the properties of the oblique waves.

The present paper investigates the properties of the oblique waves theoretically. First, the formula of waves generated by a single wave paddle is obtained theoretically. The properties of the wave height and propagating angle are analysed in detail by the computation of the formula. The distributions of the wave height show concentric features in the case of a small relative width of the paddle, while they become more complex as the width become larger. On the other hand, the contour lines of the wave propagating angle show radiative features in the case of a small relative width. The variations of the wave height and propagating angle show wavy features on the line parallel to the wave paddle. The wavy variations do not disappear, even if the paddle is widened. The validity of the formulation is confirmed by the comparison of the computed wave heights to the experimental ones.

Second, the formula of the oblique waves is obtained as the linear superposition of the above formula by controlling the phase difference between the motions of adjacent wavemakers. The formula predicts that the oblique waves generated by serpent-type wavemakers vary in their heights and propagating directions on the lines parallel to the wave paddles. The variation consists of ripple and undulation pattern, and cannot be made to disappear, even if the width of each paddle is reduced to infinitesimal value.

Finally, the effect of wave reflection from the side walls is analysed by applying the mirror image method, and some numerical results are presented.

* Chief of the Wave Laboratory, Marine Hydrodynamics Division

港湾技術研究所報告
第21巻 第2号 (1982. 6)

1. 造波機によって発生する斜め波の特性について

高 山 知 司*

要 旨

実際の海の波が方向スペクトルを有する不規則波であることはよく知られている。このような特性を有する不規則波を実験水槽内に再現し，実際の海の波に近い条件で波の変形や波と構造物の干渉の問題を研究することは非常に重要なことである。

本研究は，方向スペクトルを有する不規則波を発生させる上において重要な斜め波の特性について理論解析を行ったものである。まず，一直線上に配置された数多くの造波機のうちの一台が作動するときに発生する波の理論解を求めた。この理論解の妥当性は実験によって確認した。一枚の造波板の運動によって発生する波の解を重ね合わせることによって，斜め波の理論解を求めた。この重ね合わせにおいては，各造波板の運動の位相差を考慮している。この解を用いて，斜め波の波高変化および進行方向の変化を調べた。最後に，反射壁を有する水槽内での斜め波の特性についても，鏡像関係を用いて解析した。

本研究で得られた主要な結論は以下のとおりである。

1) 造波板の微小振幅運動を仮定して求めた，一枚の造波板で起される波の理論解は，模型実験結果とよく一致している。

2) 造波板の幅 b と波長Lとの比 b/L が 0.5 以下では，等波高線は同心円状になり，等波向線は放射状になる。しかし，b/L が大きくなると，波高および波向分布ともに非常に複雑になる。

3) 各造波板の運動の位相差を考慮して，斜め波の解を上記の解の重ね合わせとして求めた。この解を用いた解析では，斜め波の波高および波向は一様にならず，場所的に変動することがわかった。この変動は，造波板の幅を非常に小さくしても消すことができないことが判明した。

* 海洋水理部 波浪研究室長

CONTENTS

1. Introduction

An aerial photograph of sea surface exhibits the features of short crested waves, which are quite different from the waves generated by a wavemaker in a laboratory tank. The short crested waves are thought to appear as a result of the superposition of an infinite number of component waves which come from various directions. Thus, real sea waves have a property of directional randomness. The property of the directional randomness has been investigated through the analysis of field data by many researchers in the world. Consequently, several forms of the angular spreading function, which shows the wave energy distribution to wave directions, have been proposed as a standard form. The functions of Mitsuyasu[1] or Cote et al[2] are most popularly known as the functional form.

These functions are employed in many engineering applications such as estimating wave trnsformations like refraction and diffraction of random waves.[3],[4] However, the methods of the estimation have hardly been evaluated by field observations or experiments. The reasons why the evaluation has not been carried out are as follows:

1) For the evaluation by field data, it is necessary to obtain directional spectra in deep sea and shallow area. But it is very difficult to observe them simultaneously.
2) Laboratory experiments are the best ways to evaluate the accuracy of estimation methods, because the conditions can be easily simplified. Wave generators which can generate directional random waves have been invented in England, but they are available for limited number of researchers only, presently.

It is of great importance to reproduce the directional random waves in a wave tank and to use them for the experiments on interactions between waves and marine structures as well as on the above transformations.

In the Hydraulic Research Station in England, multi-directional random waves are generated by a group of ten wavemakers arranged in a crescent.[5] In this method, the directional random waves are well defined in the center area of two meters squares where uni-directional random waves are concentrated. Therefore, they are available in the experiments only for an offshore structure installed at the center, but they are not usefull in the experiments on the wave transformations, because the wave spectrum must be uniform in much broader area.

The report[6] of Edinburgh University describes that wavemakers of mixed frequency serpent-type have been built for generation of directional random waves. The principle of the wave generation is based on the linear superposition of oblique waves produced by controlling the phase difference between the signals sent to adjacent wavemakers. This is an analogy with Huygens principle in optics. The characteristics of wave directional spectrum generated by the wavemakers have not been reported in technical journals yet.

The Norwegian Hydrodynamic Laboratories have just built wavemakers for uniform generation of directional spectral waves. The principle of the wave generation are based on the natural wave diffraction.[7] Each wavemaker is operated in independent phase of motion to the adjacent one. Consequently, the principle is similar to that in the Hydraulic Research Station, but the Norwegian Hydrodynamic Laboratories expect that uniform directional spectrum can be generated in a whole basin by applying wave reflection from the basin walls.

Thus, the various techniques are employed in generation of directional random waves, but no theoretical analysis in exact sence has been presented for the wave

generation by a group of wavemakers.

In this report, a formula of waves generated by a single wave maker is derived theoretically, and the properties of the generated waves are investigated numerically. The validity of the formula is evaluated by the experiments. The formula of oblique waves is obtained as the linear superposition of the above formula by taking into consideration the phase difference between the motions of adjacent wavemakers. The variations of heights and propagating angles of the oblique waves are investigated. In an ordinary wave tank, waves are reflected from side walls of the tank. Then, the formula of oblique waves in the tank is derived by applying the mirror image method, and the characteristics of the waves are studied numerically.

2. Formulation of Waves Generated by a Single Wavemaker

2.1 Assumptions and Boundary Conditions

Before the theoretical formulation, fluid, fluid motion and boundary conditions are assumed as follows:

1) The fluid is non-viscous and incompressible.
2) The fluid motion is irrotational.
3) The water depth is uniform.
4) The displacement of a wave paddle is sufficiently small, compared to the water depth and the wave length. Consequently, the waves generated by the motion of a paddle can be regarded as small amplitude waves.
5) The bottom and the wave paddle are impermeable.

Under the above assumptions, the fluid motion can be expressed by a velocity potential Φ, which satisfies the following Laplace equation:

$$\frac{\partial^2\Phi}{\partial x^2}+\frac{\partial^2\Phi}{\partial y^2}+\frac{\partial^2\Phi}{\partial z^2}=0 \ , \tag{1}$$

where the coordinates of x and y are horizontal axes on a still water surface and the coordinate of z is a vertical axis, possitive upwards. They are shown in **Figs. 1** and **2**. The condition on water surface is given by the assumption of the small amplitude wave, as follows:

$$\left[\frac{\partial^2\Phi}{\partial t^2}+g\frac{\partial\Phi}{\partial z}\right]_{z=0}=0 \ , \tag{2}$$

where t and g denote time and acceleration of gravity, respectively. The bottom condition is expressed as

$$\left.\frac{\partial\Phi}{\partial z}\right|_{z=-h}=0 \ , \tag{3}$$

where h is the water depth.

It is assumed that a single wave paddle of b wide moves periodically to and fro in a constant amplitude and that two motionless boards are extended semi-infinitely in both sides along the line of the wave paddle, as shown in **Fig. 1**. The motion of the paddle is presumed to consist of a parallel movement and a rotational one, as shown in **Fig. 2**. The former and the latter correspond to the motions of a piston-type wavemaker and a flap-type one, respectively. The movement y_0 of the paddle at z can be expressed as the sum of them in the following form:

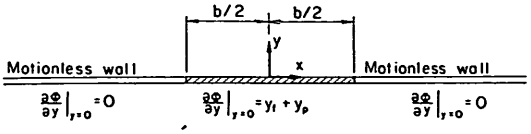

Fig. 1 Boundary conditions

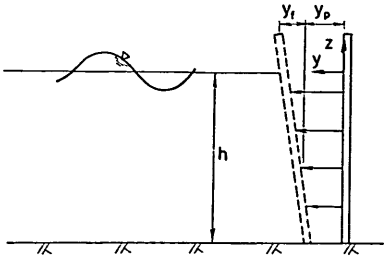

Fig. 2 Motion of a wave paddle

$$y_0 = y_p + y_f \frac{h+z}{h} \ , \tag{4}$$

where y_p and y_f are the displacements of the parallel motion and the rotational one, respectively, at the still water surface, as shown in **Fig. 2**. The boundary conditions on the wave paddle and the motionless boards are formulated as follows:

$$\left.\frac{\partial\Phi}{\partial y}\right|_{y=0} = \begin{cases} \sigma\left(Y_p + Y_f \dfrac{h+z}{h}\right)\cos\sigma t & (|x| \le b/2) \\ 0 & (|x| > b/2) \ , \end{cases} \tag{5}$$

where Y_p and Y_f are amplitudes of the motions corresponding to y_p and y_f, respectively.

Since the waves generated by the single paddle of a finite width must propagate in radiative directions and diminish their own amplitudes, they satisfy the following radiation condition[8] at a point sufficiently distant from a center of the paddle:

$$\lim_{r\to\infty} \sqrt{r}\left(\frac{\partial\Phi}{\partial r} + \frac{k}{\sigma}\frac{\partial\Phi}{\partial t}\right) = 0 \ , \tag{6}$$

where $r(=\sqrt{x^2+y^2})$ is a distance from the origin, and $k(=2\pi/L)$ and $\sigma(=2\pi/T)$ are a wave number and an angular frequency, respectively. Furthermore, L and T denote wave length and period, respectively.

2.2 Form of Velocity Potential

The velocity potential, which satisfies the bottom condition of Eq. (3), is expressed in the following form:

$$\Phi = \{\phi^c(x, y)\cos\sigma t + \phi^s(x, y)\sin\sigma t\}\cosh k(h+z) \ . \tag{7}$$

By substituting Eq. (7) into Eq. (2), the following dispersion relation of waves is derived:

$$\sigma^2 = gk\tanh kh \ . \tag{8}$$

The solution of k in Eq. (8) has a real value and infinite number of imaginary values. When the real solution and the imaginary one are represented by k and $i\nu$, respectively, k is a real solution of Eq. (8) and ν is real solution of the following equation:

$$\sigma^2=-g\nu\tan\nu h\ . \tag{9}$$

The functions of $\cosh k(h+z)$ and $\cos\nu(h+z)$ are orthogonal, as shown in the following formulas:

$$\left.\begin{aligned}
&\int_{-h}^{0}\cosh^2 k(h+z)\,dz=\frac{h}{2}\left[1+\frac{\sinh 2kh}{2kh}\right]\ ,\\
&\int_{-h}^{0}\cosh k(k+z)\cos\nu(h+z)\,dz=0\ ,\\
&\int_{-h}^{0}\cos\nu_1(h+z)\cos\nu_2(h+z)\,dz=\begin{cases}\dfrac{h}{2}\left[1+\dfrac{\sin 2\nu h}{2\nu h}\right] & (\nu_1=\nu_2=\nu)\\ 0 & (\nu_1\neq\nu_2)\ .\end{cases}
\end{aligned}\right\} \tag{10}$$

By using the above orthogonality, the velocity potential of Eq. (7) can be rewritten as

$$\begin{aligned}\Phi=&\left[\phi_k^c(x,y)\cosh k(h+z)+\sum_\nu\phi_\nu^c(x,y)\cos\nu(h+z)\right]\cos\sigma t\\&+\left[\phi_k^s(x,y)\cosh k(h+z)+\sum_\nu\phi_\nu^s(x,y)\cos\nu(h+z)\right]\sin\sigma t\ .\end{aligned} \tag{11}$$

When Eq. (11) is substituted into Eq. (1) and the above orthogonality between $\cosh k(h+z)$ and $\cos\nu(h+z)$ is applied, $\phi_k^{c,s}$ and $\phi_\nu^{c,s}$ safisty the following Helmholz equations individually:

$$\frac{\partial^2\phi_k^{c,s}}{\partial x^2}+\frac{\partial^2\phi_k^{c,s}}{\partial y^2}+k^2\phi_k^{c,s}=0\ , \tag{12}$$

$$\frac{\partial^2\phi_\nu^{c,s}}{\partial x^2}+\frac{\partial^2\phi_\nu^{c,s}}{\partial y^2}-\nu^2\phi_\nu^{c,s}=0\ . \tag{13}$$

By substituting Eq. (11) into the boundary condition of Eq. (5), the orthogonality between $\cos\sigma t$ and $\sin\sigma t$ derives the following two formulas with respect to $\phi_k^{c,s}$ and $\phi_\nu^{c,s}$:

$$\begin{aligned}&\left.\frac{\partial\phi_k^c}{\partial y}\right|_{y=0}\cosh k(h+z)+\sum_\nu\left.\frac{\partial\phi_\nu^c}{\partial y}\right|_{y=0}\cos\nu(h+z)\\&\qquad=\begin{cases}\sigma\left(Y_p+\dfrac{h+z}{h}Y_f\right) & (|x|\leq b/2)\\ 0 & (|x|>b/2)\ ,\end{cases}\end{aligned} \tag{14}$$

$$\left.\frac{\partial\phi_k^s}{\partial y}\right|_{y=0}\cosh k(h+z)+\sum_\nu\left.\frac{\partial\phi_\nu^s}{\partial y}\right|_{y=0}\cos\nu(h+z)=0\ . \tag{15}$$

By applying the orthogonality of Eq. (10) to Eqs. (14) and (15), the four boundary conditions with respect to $\phi_k^{c,s}$ and $\phi_\nu^{c,s}$ are derived as follows:

$$\left.\frac{\partial \phi_k^c}{\partial y}\right|_{y=0}=\begin{cases}\dfrac{2\sigma(Y_p\alpha_p+Y_f\alpha_f)}{\sinh kh} & (|x|\leq b/2)\\ 0 & (|x|>b/2)\end{cases}, \tag{16}$$

$$\left.\frac{\partial \phi_\nu^c}{\partial y}\right|_{y=0}=\begin{cases}\dfrac{2\sigma(Y_p\beta_p+Y_f\beta_f)}{\sin \nu h} & (|x|\leq b/2)\\ 0 & (|x|>b/2)\end{cases}, \tag{17}$$

$$\left.\frac{\partial \phi_k^s}{\partial y}\right|_{y=0}=0\ , \tag{18}$$

$$\left.\frac{\partial \phi_\nu^s}{\partial y}\right|_{y=0}=0\ , \tag{19}$$

where

$$\left.\begin{aligned}\alpha_p&=\frac{\sinh^2 kh}{kh\left[1+\dfrac{\sinh 2kh}{2kh}\right]}\ ,\\ \beta_p&=\frac{\sin^2 \nu h}{\nu h\left[1+\dfrac{\sin 2\nu h}{2\nu h}\right]}\ ,\end{aligned}\right\} \tag{20}$$

$$\left.\begin{aligned}\alpha_f&=\frac{[\sinh kh-(\cosh kh-1)/kh]\sinh kh}{kh\left[1+\dfrac{\sinh 2kh}{2kh}\right]}\ ,\\ \beta_f&=\frac{[\sin \nu h+(\cos \nu h-1)/\nu h]\sin \nu h}{\nu h\left[1+\dfrac{\sin 2\nu h}{2\nu h}\right]}\ .\end{aligned}\right\} \tag{21}$$

2.3 Cosine Transformation on a Half Line

Since the boundary conditions shown in **Fig. 2** are symmetrical to y-axis, each functional forms of $\phi_k^{c,s}$ and $\phi_\nu^{c,s}$ must become odd functions with respect to x. Therefore, the following cosine transformation on a half line[9] of possitive x is performed to $\phi_k^{c,s}$ and $\phi_\nu^{c,s}$:

$$\left.\begin{aligned}\bar{\phi}_k^{c,s}&=\int_0^\infty \phi_k^{c,s}\cos \lambda x\, dx\ ,\\ \bar{\phi}_\nu^{c,s}&=\int_0^\infty \phi_\nu^{c,s}\cos \lambda x\, dx\ .\end{aligned}\right\} \tag{22}$$

If the functions of $\bar{\phi}_k^{c,s}$ and $\bar{\phi}_\nu^{c,s}$ are obtained, $\bar{\phi}_k^{c,s}$ and $\bar{\phi}_\nu^{c,s}$ are given by the inverse transformation as

$$\left.\begin{aligned}\phi_k^{c,s}&=\frac{2}{\pi}\int_0^\infty \bar{\phi}_k^{c,s}\cos \lambda x\, d\lambda\ ,\\ \phi_\nu^{c,s}&=\frac{2}{\pi}\int_0^\infty \bar{\phi}_\nu^{c,s}\cos \lambda x\, d\lambda\ .\end{aligned}\right\} \tag{23}$$

When $\cos \lambda x$ is multiplied to both sides of Eqs. (12) and (13) and the two equa-

tions are integrated with respect to x from 0 to possitive infinity, they are transformed as follows:

$$\frac{\partial^2\bar{\phi}_k^{c,s}}{\partial y^2}+(k^2-\lambda^2)\bar{\phi}_k^{c,s}=0\ , \tag{24}$$

$$\frac{\partial^2\bar{\phi}_\nu^{c,s}}{\partial y^2}-(\nu^2+\lambda^2)\bar{\phi}_\nu^{c,s}=0\ . \tag{25}$$

Furthermore, the integration in same manner as the above for the boundary equations of Eqs. (16) to (19) derives the following equations:

$$\left.\frac{\partial\bar{\phi}_k^c}{\partial y}\right|_{y=0}=\frac{2\sigma(Y_p\alpha_p+Y_f\alpha_f)}{\sinh kh}\frac{\sin(\lambda b/2)}{\lambda}\ , \tag{26}$$

$$\left.\frac{\partial\bar{\phi}_\nu^c}{\partial y}\right|_{y=0}=\frac{2\sigma(Y_p\beta_p+Y_f\beta_f)}{\sinh \nu h}\frac{\sin(\lambda b/2)}{\lambda}\ , \tag{27}$$

$$\left.\frac{\partial\bar{\phi}_k^s}{\partial y}\right|_{y=0}=0\ , \tag{28}$$

$$\left.\frac{\partial\bar{\phi}_\nu^s}{\partial y}\right|_{y=0}=0\ . \tag{29}$$

The solution of Eq. (24) is given in the following form:

$$\bar{\phi}_k^{c,s}=\begin{cases} A^{c,s}\exp[-y\sqrt{\lambda^2-k^2}]+B^{c,s}\exp[y\sqrt{\lambda^2-k^2}] & (\lambda>k) \\ C^{c,s}\cos[y\sqrt{k^2-\lambda^2}]+D^{c,s}\sin[y\sqrt{k^2-\lambda^2}] & (\lambda\leq k)\ , \end{cases} \tag{30}$$

where $A^{c,s}$, $B^{c,s}$, $C^{c,s}$ and $D^{c,s}$ are unknown functions of λ which are determined later by the boundary conditions and the radiation condition.

The substitution of $\bar{\phi}_k^c$ of Eq. (30) into the boundary condition of Eq. (26) derives the following relations among the unknown functions:

$$\left.\begin{aligned} A^c&=B^c-\frac{2\sigma(Y_p\alpha_p+Y_f\alpha_f)}{\sinh kh}\frac{\sin(b\lambda/2)}{\lambda}\frac{1}{\sqrt{\lambda^2-k^2}}\ , \\ D^c&=\frac{2\sigma(Y_p\alpha_p+Y_f\alpha_f)}{\sinh k\lambda}\frac{\sin(\lambda b/2)}{\lambda}\frac{1}{\sqrt{k^2-\lambda^2}}\ . \end{aligned}\right\} \tag{31}$$

The function of $\bar{\phi}_k^c$ must be finite even at infinitely large value of y, as implied in the radiation condition of Eq. (60). Then,

$$B^c=0\ . \tag{32}$$

Consequently, the form of $\bar{\phi}_k^c$ is given as follows:

$$\bar{\phi}_k^c=\begin{cases} -2\sigma\dfrac{(Y_p\alpha_p+Y_f\alpha_f)}{\sinh kh}\dfrac{\sin(\lambda b/2)}{\lambda}\dfrac{\exp[-y\sqrt{\lambda^2-k^2}]}{\sqrt{\lambda^2-k^2}} & (\lambda>k) \\ 2\sigma\dfrac{(Y_p\alpha_p+Y_f\alpha_f)}{\sinh kh}\dfrac{\sin(\lambda b/2)}{\lambda}\dfrac{\sin[y\sqrt{k^2-\lambda^2}]}{\sqrt{k^2-\lambda^2}}+C^c\cos[y\sqrt{k^2-\lambda^2}] & (\lambda\leq k)\ . \end{cases} \tag{33}$$

In the same manner, the functions of $\bar{\phi}_\nu^c$, $\bar{\phi}_k^s$, and $\bar{\phi}_\nu^s$ are obtained as

$$\tilde{\phi}_\nu^c = -2\sigma \frac{(Y_p\beta_p + Y_f\beta_f)}{\sin \nu h} \frac{\sin(\lambda b/2)}{\lambda} \frac{\exp[-y\sqrt{\lambda^2+\nu^2}]}{\sqrt{\lambda^2+\nu^2}} , \tag{34}$$

$$\tilde{\phi}_k^s = \begin{cases} 0 & (\lambda > k) \\ C^s \cos[\sqrt{k^2-\lambda^2}\, y] & (\lambda \leq k) , \end{cases} \tag{35}$$

$$\tilde{\phi}_\nu^s = 0 . \tag{36}$$

Since Eqs. (33) and (35) include unknown functions of C^c and C^s, it is necessary to determine the forms of them. The velocity potential Φ must satisfy the radiation condition of Eq. (6), which means that the generated waves become progressive at sufficiently large value of r. The transformed velocity potencial is also necessary to satisfy the following transformed radiation condition at a sufficiently large value of y:

$$\frac{\partial \tilde{\Phi}}{\partial y} + \frac{\sqrt{k^2-\lambda^2}}{\sigma} \frac{\partial \tilde{\Phi}}{\partial t} = 0 . \tag{37}$$

The transformed velocity potential is given as

$$\tilde{\Phi} = \left[\tilde{\phi}_k^c \cosh k(h+z) + \sum_\nu \tilde{\phi}_\nu^c \cos \nu(h+z) \right] \cos \sigma t + \tilde{\phi}_k^s \cosh k(h+z) \sin \sigma t . \tag{38}$$

However, the second term in [ ] of the right hand side of Eq. (38) is unnecessary in the relation of Eq. (37), because it inverse-exponentially decreases in its value as y becomes large, and vanishes at large value of y. By substituting $\tilde{\Phi}$ of Eq. (38) into Eq. (37) without the second term, the unknown functions of C^c and C^s in Eqs. (33) and (35) are obtained as

$$\left.\begin{aligned} C^c &= 0 , \\ C^s &= -2\sigma \frac{(Y_p\alpha_p + Y_f\alpha_f)}{\sinh kh} \frac{\sin(\lambda b/2)}{\lambda} \frac{1}{\sqrt{k^2-\lambda^2}} . \end{aligned}\right\} \tag{39}$$

Consequently, $\tilde{\phi}_k^c$ and $\tilde{\phi}_k^s$ is determined completely and given as

$$\tilde{\phi}_k^c = \begin{cases} -2\sigma \dfrac{(Y_p\alpha_p + Y_f\alpha_f)}{\sinh hk} \dfrac{\sin(\lambda b/2)}{\lambda} \dfrac{\exp[-y\sqrt{\lambda^2-k^2}]}{\sqrt{\lambda^2-k^2}} & (\lambda > k) \\ 2\sigma \dfrac{(Y_p\alpha_p + Y_f\alpha_f)}{\sinh kh} \dfrac{\sin(\lambda b/2)}{\lambda} \dfrac{\sin[y\sqrt{k^2-\lambda^2}]}{\sqrt{k^2-\lambda^2}} & (\lambda \leq k) , \end{cases} \tag{40}$$

$$\tilde{\phi}_k^s = \begin{cases} 0 & (\lambda > k) \\ -2\sigma \dfrac{(Y_p\alpha_p + Y_f\alpha_f)}{\sinh kh} \dfrac{\sin(\lambda b/2)}{\lambda} \dfrac{\cos[y\sqrt{k^2-\lambda^2}]}{\sqrt{k^2-\lambda^2}} & (\lambda \leq k) . \end{cases} \tag{41}$$

2.4 Solution of Velocity Potential

Since the cosine transformed functions of $\tilde{\phi}_k^c$, $\tilde{\phi}_k^s$, $\tilde{\phi}_\nu^c$ and $\tilde{\phi}_\nu^s$ have been determined, the velocity potential can be derived by the inverse transformation shown in Eq. (23). In the inverse transformation, the following relation is useful when $F(x)$ and $G(x)$ are odd functions:

$$\int_0^\infty F(x)\{G(x-p)+G(x+p)\}dp=\frac{2}{\pi}\int_0^\infty 2\tilde{F}(\lambda)\tilde{G}(\lambda)\cos\lambda x\,d\lambda\ , \tag{42}$$

where

$$\left.\begin{aligned}\tilde{F}(\lambda)&=\int_0^\infty F(x)\cos\lambda x\,dx\ ,\\ \tilde{G}(\lambda)&=\int_0^\infty G(x)\cos\lambda x\,dx\ .\end{aligned}\right\} \tag{43}$$

The cosine transforms of various functions are tabulated in the reference 10). The transforms necessary in the analysis are picked up from the table and written down in the below.

$$\left.\begin{aligned}&\frac{2}{\pi}\int_0^\infty\frac{\sin(\lambda b/2)}{\lambda}\cos\lambda x\,d\lambda=\begin{cases}1 & (0\le x\le b/2)\\ 0 & (x>b/2)\end{cases}\ ,\\ &\frac{2}{\pi}\int_0^k\frac{\cos[y\sqrt{k^2-\lambda^2}]}{\sqrt{k^2-\lambda^2}}\cos\lambda x\,d\lambda=J_0(k\sqrt{x^2+y^2})\ ,\\ &\frac{2}{\pi}\left\{\int_0^k\frac{\sin[y\sqrt{k^2-\lambda^2}]}{\sqrt{k^2-\lambda^2}}\cos\lambda x\,d\lambda-\int_k^\infty\frac{\exp[-y\sqrt{\lambda^2-k^2}]}{\sqrt{\lambda^2-k^2}}\cos\lambda x\,d\lambda\right\}\\ &\qquad=N_0(k\sqrt{x^2+y^2})\ ,\\ &\frac{2}{\pi}\int_0^\infty\frac{\exp[-y\sqrt{\lambda^2+\nu^2}]}{\sqrt{\nu^2+\lambda^2}}\cos\lambda x\,d\lambda=\frac{2}{\pi}K_0(\nu\sqrt{x^2+y^2})\ ,\end{aligned}\right\} \tag{44}$$

where $J_0(x)$, $N_0(x)$ and $K_0(x)$ are Bessel, Neumann and modified Bessel functions with index zero, respectively.

By applying the relation of Eq. (42) to the inverse transformation of Eq. (40), the function of ϕ_k^c is given as follows:

$$\phi_k^c=\frac{\sigma(Y_p\alpha_p+Y_f\alpha_f)}{\sinh kh}\int_0^{b/2}\{N_0(k\sqrt{(x-p)^2+y^2})+N_0(k\sqrt{(x+p)^2+p^2})\}\,dp\ . \tag{45}$$

By replacement of p by q/k and arrangement of Eq. (45), the above equation is re-written as follows:

$$\phi_k^c=\frac{\sigma}{k}\frac{(Y_p\alpha_p+Y_f\alpha_f)}{\sinh kh}\int_{-kb/2}^{kb/2}N_0(\sqrt{(kx-q)^2+(ky)^2})\,dq\ . \tag{46}$$

In the same manner, ϕ_ν^c, ϕ_k^s, and ϕ_ν^s are given as

$$\phi_\nu^c=-\frac{\sigma}{\nu}\frac{(Y_p\beta_p+Y_f\beta_f)}{\sin\nu h}\int_{-\nu b/2}^{\nu b/2}\frac{2}{\pi}K_0(\sqrt{(\nu x-q)^2+(\nu y)^2})\,dq\ , \tag{47}$$

$$\phi_k^s=-\frac{\sigma}{k}\frac{(Y_p\alpha_p+Y_f\alpha_f)}{\sinh kh}\int_{-kb/2}^{kb/2}J_0(\sqrt{(kx-q)^2+(ky)^2})\,dq\ , \tag{48}$$

$$\phi_\nu^s=0\ . \tag{49}$$

By substitution of ϕ_k^c, ϕ_ν^c, ϕ_k^s and ϕ_ν^s into Eq. (11), the velocity potential is given as

$$\Phi=\left[\frac{\sigma}{k}(Y_p\alpha_p+Y_f\alpha_f)\frac{\cosh k(h+z)}{\sinh kh}\int_{-kb/2}^{kb/2}N_0(\sqrt{(kx-q)^2+(ky)^2})\,dq\right.$$
$$\left.-\sum_\nu\frac{\sigma}{\nu}(Y_p\beta_p+Y_f\beta_f)\frac{\cos\nu(h+z)}{\sin\nu h}\int_{-\nu b/2}^{\nu b/2}\frac{2}{\pi}K_0(\sqrt{(\nu x-q)^2+(\nu y)^2})\,dq\right]$$
$$\times\cos\sigma t-\frac{\sigma}{k}(Y_p\alpha_p+Y_f\alpha_f)\frac{\cosh k(h+z)}{\sinh kh}\sin\sigma t$$
$$\times\int_{-kb/2}^{kb/2}J_0(\sqrt{(kx-q)^2+(ky)^2})\,dq\ . \tag{50}$$

3. Properties of Waves Generated by a Single Wavemaker

3.1 Stationary Wave Term and Dimensionless of Wave Height

The water surface displacement η is given by the Bernoulli equation for small amplitude waves as

$$\eta=-\frac{1}{g}\frac{\partial\Phi}{\partial t}\bigg|_{z=0}\ . \tag{51}$$

By substituting the velocity potential of Eq. (50) into Eq. (51) and by using the dispersion relations of Eqs. (8) and (9), Eq. (51) is rewritten as

$$\eta=\left[(Y_p\alpha_p+Y_f\alpha_f)\int_{-kb/2}^{kb/2}N_0(\sqrt{(kx-q)^2+(ky)^2})\,dq\right.$$
$$\left.+\sum_\nu(Y_p\beta_p+Y_f\beta_f)\int_{-\nu b/2}^{\nu b/2}\frac{2}{\pi}K_0(\sqrt{(\nu x-q)^2+(\nu y)^2})\,dq\right]\sin\sigma t$$
$$+(Y_p\alpha_p+Y_f\alpha_f)\cos\sigma t\int_{-kb/2}^{kb/2}J_0(\sqrt{(kx-q)^2+(ky)^2})\,dq\ . \tag{52}$$

In order to clarify the properties of η, the expression of η may well be reformed as follows:

$$\eta=A(x,y)\cos\{l(x,y)-\sigma t\}$$
$$+\sum_\nu(Y_p\beta_p+Y_f\beta_f)\sin\sigma t\int_{-\nu b/2}^{\nu b/2}\frac{2}{\pi}K_0(\sqrt{(\nu x-q)^2+(\nu y)^2})\,dq\ , \tag{53}$$

where

$$A(x,y)=(Y_p\alpha_p+Y_f\alpha_f)\left[\left\{\int_{-kb/2}^{kb/2}N_0\sqrt{(kx-q)^2+(ky)^2})\,dq\right\}^2\right.$$
$$\left.+\left\{\int_{-kb/2}^{kb/2}J_0(\sqrt{(kx-q)^2+(ky)^2})\,dq\right\}^2\right]^{1/2}\ , \tag{54}$$

and

$$l(x,y)=\arctan\left\{\int_{-kb/2}^{kb/2}N_0(\sqrt{(kx-q)^2+(ky)^2})\,dq\right.$$
$$\left./\int_{kb/2}^{kb/2}J_0(\sqrt{(kx-q)^2+(ky)^2})\,dq\right\}\ . \tag{55}$$

The first term in the right hand side of Eq. (53) represents a progressive wave

which propagates outerwards, decreasing in its height gradually. On the other hand, the second term in the same side represents a stationary wave which is not progressive and deminishes its own height inverse-exponentially as its location becomes distant from the origin. Consequently, it can be guessed that the second term becomes negligible at a point a little distant from the paddle.

In order to investigate the degree of the influence of the stationary wave term to the water surface displacement, the comparison between the dimensionless wave heights with and without the term is made for the piston-type wavemaker, for which $Y_f=0$. The dimensionless wave height is expressed as the ratio to the stroke of the wave paddle in the following formula:

$$\frac{H}{2Y_p}=\left[\left\{\alpha_p\int_{-kb/2}^{kb/2}N_0(\sqrt{(kx-q)^2+(ky)^2})\,dq+\sum_\nu\beta_p\int_{-kb/2}^{kb/2}\frac{2}{\pi}K_0(\sqrt{(kx-q)^2+(ky)^2})\,dq\right\}^2+\left\{\alpha_p\int_{-kb/2}^{kb/2}J_0(\sqrt{(kx-q)^2+(ky)^2})\,dq\right\}^2\right]^{1/2}, \tag{56}$$

where H denotes the wave height which is twice amplitude of η.

The above comparison is shown in **Figs. 3** and **4**, in which the solid line and broken one represent the dimensionless wave height with and without the term, respectively. **Figures 3** and **4** are for a narrow paddle width of 1 m and a broad one of 20 m, respectively. In these figures, it is clarified that the stationary term becomes less influential as a point becomes more distant from the center of the paddle, but that its influence spreads in wider region as the width of the paddle becomes larger. In any way, the term becomes neglegible at the point of y/L more than 1.0. The waves near the wave paddle are not important in the report. Therefore, it is no problem to ignore the stationary term. Hereafter, the analysis is carried out in the ignorance of the stationary term. By ignoring the term, the dimensionless wave height R_H is defined as follows:

$$R_H=\frac{H}{2(Y_p\alpha_p+Y_f\alpha_f)}=\left[\left\{\int_{-kb/2}^{kb/2}J_0(\sqrt{(kx-q)^2+(ky)^2})\,dq\right\}^2+\left\{\int_{-kb/2}^{kb/2}N_0(\sqrt{(kx-q)^2+(ky)^2})\,dq\right\}^2\right]^{1/2}. \tag{57}$$

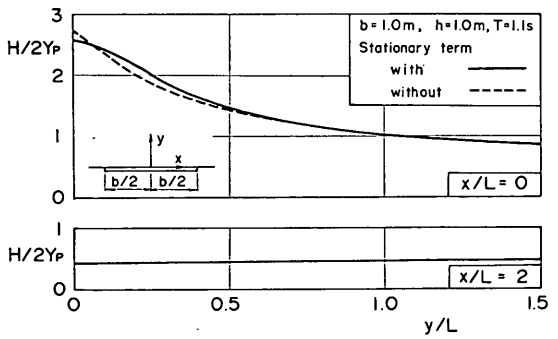

Fig. 3 Comparison between wave heights with and without the stationary wave term for b of 1 m

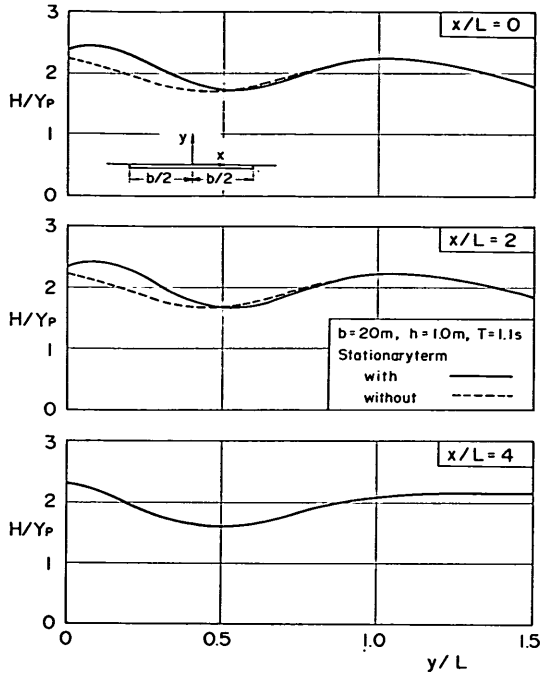

Fig. 4 Comparison between wave heights with and without the stationary wave term for b of 20 m

In the above definition of the dimensionless wave height, R_H becomes a function of b/L, x/L, and y/L and independent from h/L, Y_p and Y_f. If the value of R_H is given, the wave height is obtained in the case of the piston-type wave generator as follows:

$$H=2Y_p\alpha_p R_H \ , \tag{58}$$

and in the case of the flap-type one as follows:

$$H=2Y_f\alpha_f R_H \ . \tag{59}$$

Therefore, the definition of R_H by Eq. (57) is very convenient in the calculation of waves. The variations of α_p and α_f to relative depth h/L are shown in **Fig. 5** for convenience to the calculation of wave height. Both values of α_p and α_f converge to 1.0 as h/L becomes large, but $\alpha_p > \alpha_f$. They indicate efficiency of the wave generation by a single wave paddle and coincide with those given by Biesel et al.[11] for two-dimensional wave channel.

3.2 Definition of Wave Propagating Angle

In order to investigate the properties of waves generated by a single wavemaker, the propagating direction of the waves must be known at each point. There will be two methods in definition of the wave direction: one is to define it as a direction normal to a wave front line, and the other is to do as a direction of maximum fluid velocity. Since it is difficult in the former definition to draw wave front lines, the latter one is adopted.

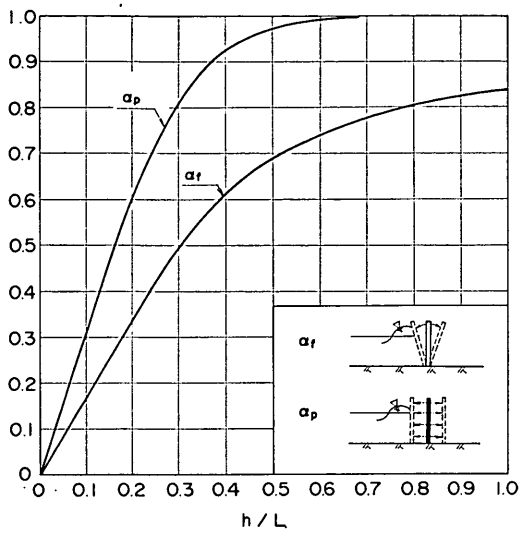

Fig. 5 Variations of α_p and α_f

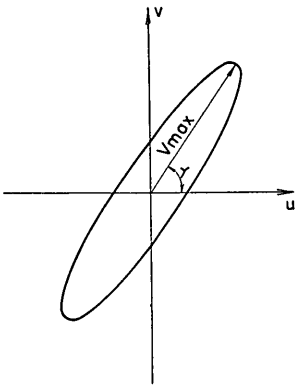

Fig. 6 Definition of wave propagating direction

The fluid velocities are given by the definition of the velocity potential as follows:

$$u=\frac{\partial \Phi}{\partial x}, \qquad v=\frac{\partial \Phi}{\partial y}, \tag{60}$$

where u and v denote the fluid velocities in the directions of x- and y-axis, respectively.

By ignoring the stationary wave term in Eq. (50) and by substituting Eq. (50) into Eq. (60), the fluid velocities of u and v are expressed as follows:

$$\begin{aligned} u=\sigma(Y_p\alpha_p+Y_f\alpha_f)\frac{\cosh k(h+z)}{\sinh kh}\Big[\cos\sigma t \\ \times\Big\{N_0(k\sqrt{(x+b/2)^2+y^2})-N_0(k\sqrt{(x-b/2)^2+y^2})\Big\} \\ -\sin\sigma t\Big\{J_0(k\sqrt{(x+b/2)^2+y^2})-J_0(k\sqrt{(x-b/2)^2+y^2})\Big\}\Big], \end{aligned} \tag{61}$$

$$\begin{aligned} v=\sigma(Y_p\alpha_p+Y_f\alpha_f)\frac{\cosh k(h+z)}{\sinh kh} \\ \times\Big[\sin\sigma t\int_{-kb/2}^{kb/2}\frac{ky}{\sqrt{(kx-q)^2+(ky)^2}}J_1(\sqrt{(kx-q)^2+(ky)^2})\,dq \\ -\cos\sigma t\int_{-kb/2}^{kb/2}\frac{ky}{\sqrt{(kx-q)^2+(ky)^2}}N_1(\sqrt{(kx-q)^2+(ky)^2})\,dq\Big], \end{aligned} \tag{62}$$

where $J_1(x)$ and $N_1(x)$ are Bessel and Neumann functions with index one, respectively.

In Eq. (61), $u=0$ at $x=0$ and $u_{x>0}=-u_{x<0}$. The velocity of u is an even function with respect to x.

The orbital curve of the composed velocity V in a wave period is shown in **Fig. 6**, where $V=\sqrt{u^2+v^2}$. A phase difference between u and v appears as shown in the figure. Therefore, when u become maximum, v is not at maximum. Thus, it is diffi-

cult to determine the wave direction, because the direction of V depends upon time. The wave propagating direction is defined as a directional angle γ at the maximum V_{max} of V as shown in **Fig. 6**.

$$\gamma=\pi/2-\arctan\{(u)_{max}/(v)_{max}\}\ , \tag{63}$$

where $(u)_{max}$ and $(v)_{max}$ denote the components of V_{max} in x- and y-direction respectively, and $(v)_{max}$ has a possitive value. The definition defines the wave direction as that of outward progressive waves.

3.3 Characteristics of Wave Height and Propagating Angle

The dimensionless wave height R_H and the wave propagating angle γ depend on the relative width b/L and the relative location of $(x/L,\ y/L)$, as shown in Eqs. (57) and (63). Then, the distributions of R_H and γ in the front area of the wave paddle are computed for various values of b/L.

The distributions of R_H and γ are shown in **Figs. 7** to **11**, where they are drafted in the area of positive x-axis, because they are symmetrical to y-axis. In **Fig. 7** for b/L of 0.05, each contour line of R_H shows a feature of a curve similar to an arc of a concentric circle, which means that R_H has equal value at a point of same distance from the center of the paddle. The values of R_H are 0.1, 0.07, 0.06 and 0.05 near 1, 2, 3 and 4 of r/L, respectively, where r is the distance from the origin of the coordinates. The tendency of the decrease shows that the value of R_H is inversely proportional to the root of r. On the other hand, the contour lines of γ are emitted in all directions from

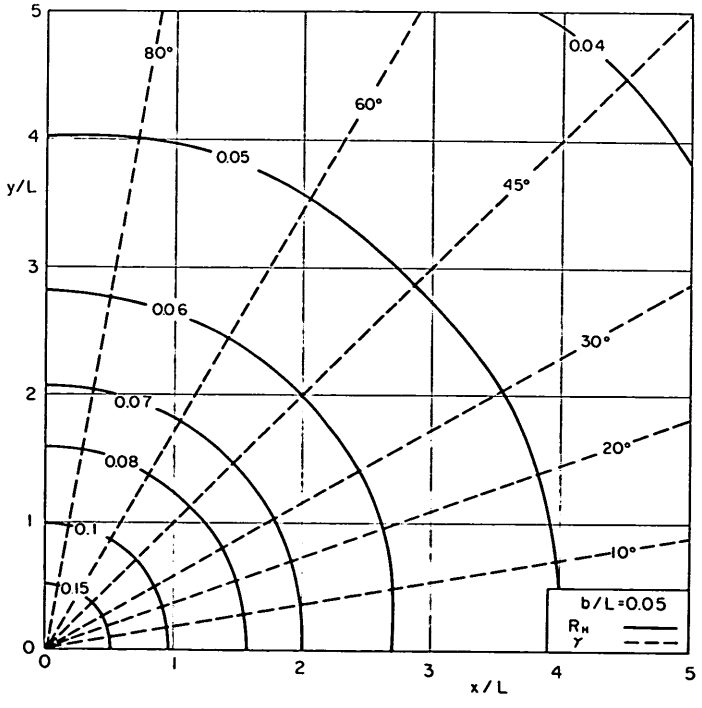

Fig. 7 Distributions of dimensionless wave height and propagating angle $(b/L=0.05)$

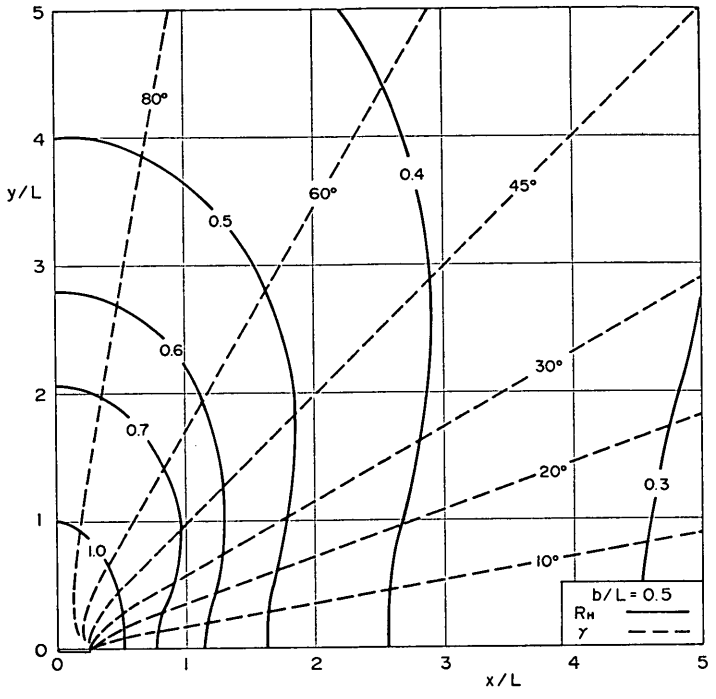

Fig. 8 Distributions of dimensionless wave height and propagating angle ($b/L=0.5$)

the center of the paddle. The values of γ agree quite well with the angle γ_p calculated by the following equation:

$$\gamma_p=\arctan(y/x) \ . \tag{64}$$

The contour lines of γ cross almost perpendicularly to those of R_H. From this fact, it is concluded that the waves generated by a paddle of a very small relative width propagate in the radial directions, decreasing in their heights in the inverse proportion to $\sqrt{r}$.

In **Fig. 8** for b/L of 0.5, the contour lines of R_H show a feature of an oval arc different from the concentric arc in **Fig. 6**. The values of R_H become larger because the relative width of b/L has increased to 0.5. The oval arc of R_H is caused by the concentration of the wave energy just in front of the paddle. Consequently, the value of R_H does not decrease in inverse proportion to $\sqrt{r}$ inside the area of **Fig. 8**. However, the value of R_H is expected to decrease in inverse proportion to $\sqrt{r}$ in the area broader than that of **Fig. 8**, judging from the distribution of R_H in **Fig. 7**. On the other hand, the contour lines of γ show radiative figures same as those in **Fig. 7** except the vicinity of the paddle. The value of γ agrees well with the angle γ_p calculated by Eq. (64), except the vicinity. In the vicinity, the lines of γ are curved toward a tip of the wave paddle. The lines of γ do not cross perpendicularly to those of R_H. This implies that the wave heights along concentric arc are not uniform, though the wave fronts draw the arc except the vicinity.

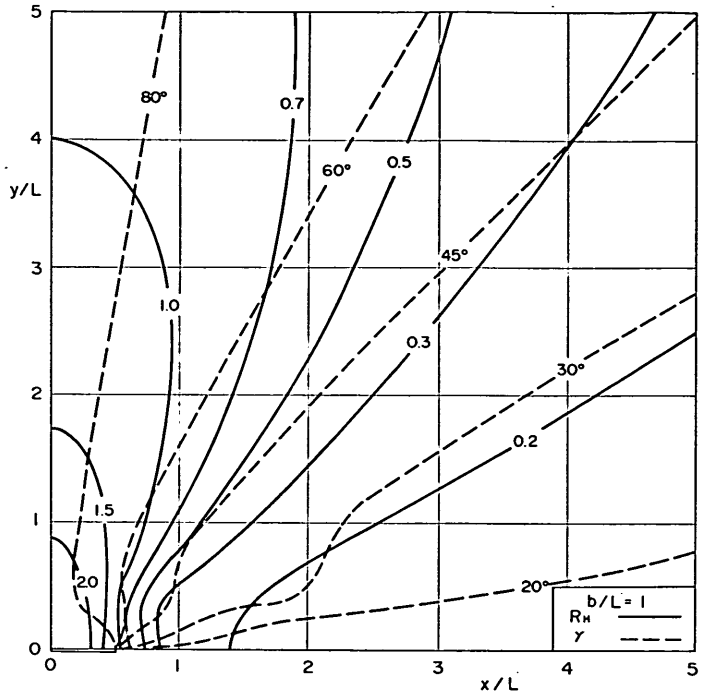

Fig. 9 Distributions of dimensionless wave height and propagating angle ($b/L=1.0$)

In **Fig. 9**, the relative width of b/L is 1. The wave energy becomes more concentrated in the front area of the paddle than in **Fig. 8**, and the value of R_H becomes larger than that of **Fig. 8** because of the increase of b/L. In **Fig. 9**, the contour lines of R_H more than 0.7 draw the curves similar to the arcs of slender ellipsises, but the lines of R_H less than 0.5 show radiative tendency. The tendency of the radiation is due to the narrowness of the area shown in **Fig. 9**, and if we compute the distribution of R_H in much broader area, each contour line will draw oval curve in the area distant from the paddle. This can be predicted by Eq. (57). The lines of γ in **Fig. 9** except the vicinity of the paddle show radiative feature as well as those in **Figs. 7** and **8**. In the vicinity, the lines turn towards the tip of the paddle and concentrate at it. The lines of γ cross those of R_H with sharp angles and the line of 30° is almost parallel to that of 0.2 in the region of x/L more than 3. The value of γ a little bit differs from the angle γ_p calculated by Eq. (64), but in the portion of straight line except the vicinity of the paddle, the slope angle of the line agrees well with the value of γ. It is drawn that though the waves propagate along the lines of γ except the vicinity, the wave height along the wave front line shows a greater variation.

In **Fig. 10** for b/L of 1.5, the value of R_H shows quite different distribution from the previous ones in **Figs. 7** to **9**. In the previous figures, the value of R_H gradually decreases on the line parallel to x-axis, as x/L becomes large. In **Fig. 10**, however, the value of R_H shows a wavy feature on the line. For example, on the line of y/L of 2, R_H gradually decreases in its value as x/L increase, and has minimum value of about 0.19 at x/L of 2. It begins to increase from the point and has maximum of about 0.3

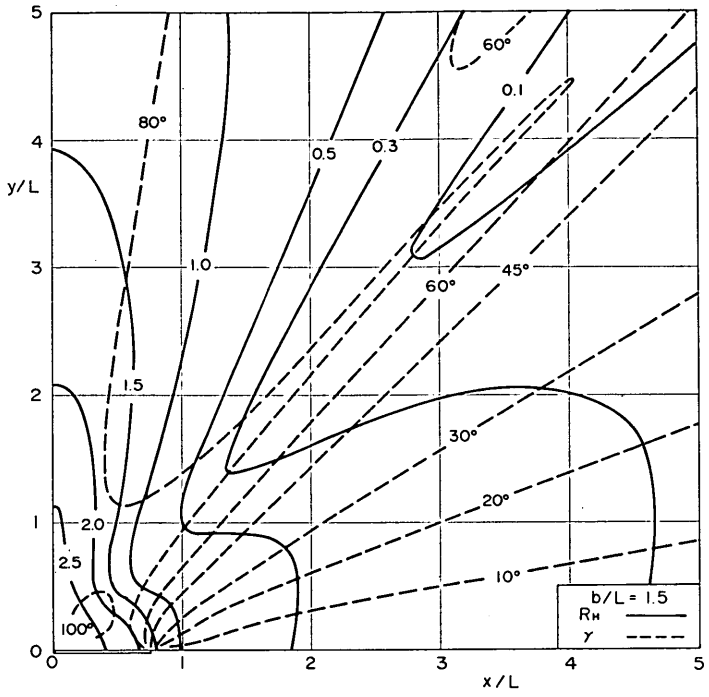

Fig. 10 Distributions of dimensionless wave height and propagating angle ($b/L=1.5$)

at x/L of 3.5. It again decreases as x/L becomes larger. This wavy pattern makes the distribution of R_H very complex. In the distribution of γ, two lines of 60° and 80° especially show very complicate pattern, but the other lines show radiative feature. In the neighborhood of the paddle, the contour line of 100° appears. The waves in the area surrounded by the line of 100° propagate in the direction of negative x-axis. The wave propagating angle γ in the figure is fairly different from the angle γ_p calculated by Eq. (64), but the slope angles of the lines other than those of 60° and 80° show good agreement with the values of γ. For example, the angle γ_p at a point of (4, 3.4) on the line of 45° is calculated by Eq. (64) as follows:

$$\gamma_p=\arctan(3.4/4)=40.4\ .$$

The difference becomes 4.6° between γ and γ_p, but the slope angle of the line is as same as 45°. Therefore, the wave propagating angle can be calculated no longer by Eq. (64), but the waves propagate along the lines of γ other than 80° and 60°.

In **Fig. 11** for b/L of 2, the feature of the distribution of R_H is almost similar to that in **Fig. 10**, though an insular line of 2.5 appears in **Fig. 11**. The values of R_H become larger than those in **Fig. 10** because of larger value of b/L. The wavy feature of R_H on the line parallel to x-axis becomes more distinguishable than that in **Fig. 10**. In the distribution of γ, the area of γ more than 80° becomes broader. The slope angles of the lines agree well with the values of γ except the lines of γ more than 80°. This means that waves propagate along the lines of γ less than 80°.

By the previous investigation of **Figs. 7** to **11**, it has been clarified that wave height

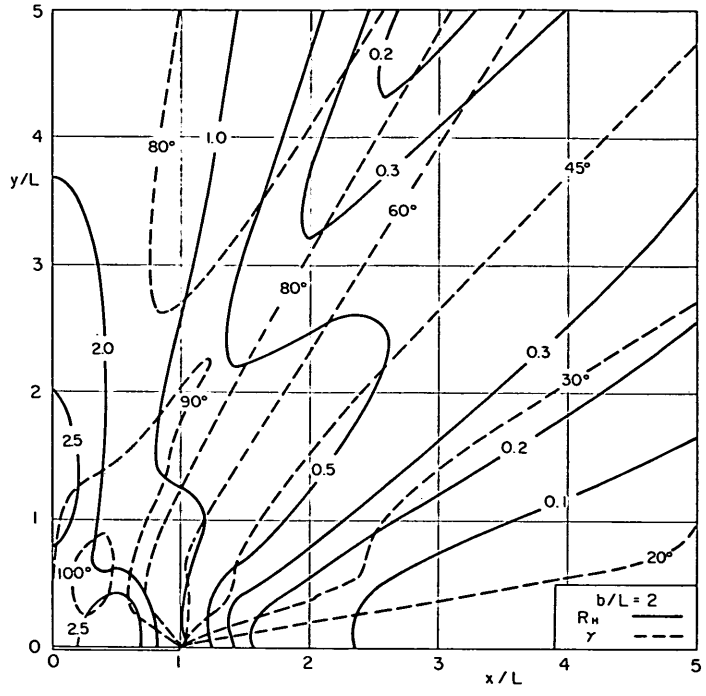

Fig. 11 Distributions of dimensionless wave height and propagating angle ($b/L=2.0$)

on the line parallel to x-axis draws a wavy variation for the value of b/L larger than 1.5. The variation of the dimensionless wave height R_H on the lines of various values of y/L is shown in **Fig. 12**. In the figure, the values of y/L are 4, 8 and 16, and b/L is 12.8. A end line of the paddle is represented by a dash-dot line.

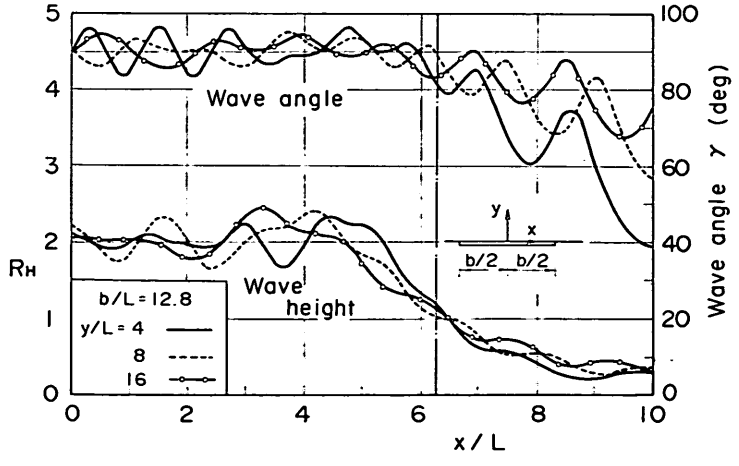

Fig. 12 Variations of wave height and wave propagating angle on the lines parallel to x-axis

As shown in the figure, both R_H and γ draw wavy variations. In the portion of x/L less than 4, the variation of R_H tends to become larger as y/L increases. On the other hand, the variation of γ becomes smaller in the portion, as the line of y/L becomes more distant from the paddle. However, the average values of R_H and γ are 2.0 and 90° in the portion, respectively. They are almost same as the values in two-dimensional wave channel. Showing a wavy variation, the value of R_H gradually decreases as x/L becomes larger than 4.3 on y/L of 4, 4.2 on y/L of 6, and 3.3 on y/L of 16. Thus, the portion of the decrease of R_H shifts inwards as the line of y/L become more distant. The inward shift is caused by outerward flow of wave energy. The outward flow increases the value of R_H in the right side of the dash-dot line, as y/L becomes larger. Showing a great wavy variation, the line of the wave propagating angle γ also shifts upwards as the line of y/L moves farther. In the figure, the variations of R_H and γ show wavy features inspite of large value of b/L like 12.8. It is predicted that their wavy variations come to disappear, and R_H and γ become uniform in large values of b/L.

The change of the variations of R_H and γ is investigated by the computation for various values of b/L. The results of the computation for y/L of 5 are shown in **Fig. 13**.

In the case of b/L of 3.2, the value of R_H represented in the solid line gradually goes down as x/L becomes larger. Showing a great variation, the wave propagating angle γ also goes down in the portion of x/L larger than 1.6. The decrease of R_H and γ is due to the small value of b/L. On the dash lines for b/L of 16, the decrease mentioned for b/L of 3.2 does not appear in the computed portion. R_H and γ of the dash lines show wavy features and the wavy variations grow larger as x/L approaches the end of the paddle. The mean values of R_H and γ are 2.0 and 90°, respectively. Even in the large value of b/L of 64, the wavy features of R_H and γ are held, but the amplitudes of the wavy variation for b/L of 64 become smaller than those for b/L of 16. Therefore, it can be predicted that the wavy variations of R_H and γ become uniform, as b/L approaches infinitely large value.

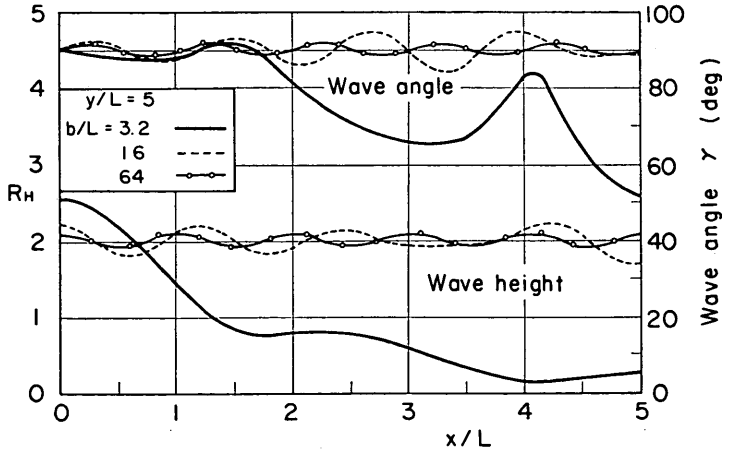

Fig. 13 Variations of wave height and wave propagating angle against b/L

4. Evaluation of Theoretical Formula by Experiments

4.1 Wave Tank and Equipments for Wave Measurement

Experiments have been carried out to evaluate the theoretical formula obtained in the previous chapter of **3**. A wave tank used for the experiments is shown in **Fig. 14**. The tank is 25 m long, 15 m wide, and 1 m high. Rubble mound and wave absorbers are placed along the tank walls to prevent waves from being reflected from the walls. The slope of the rubble mound is 1 to 5 and the wave absorbers are made of wire gauze in multiple layers.

Three wave generators of piston-type are installed in the end of the tank. Each of them has a wave paddle of 5 m wide, and can be operated simultaneously or independently. In the experiments, a central wave generator only has been operated

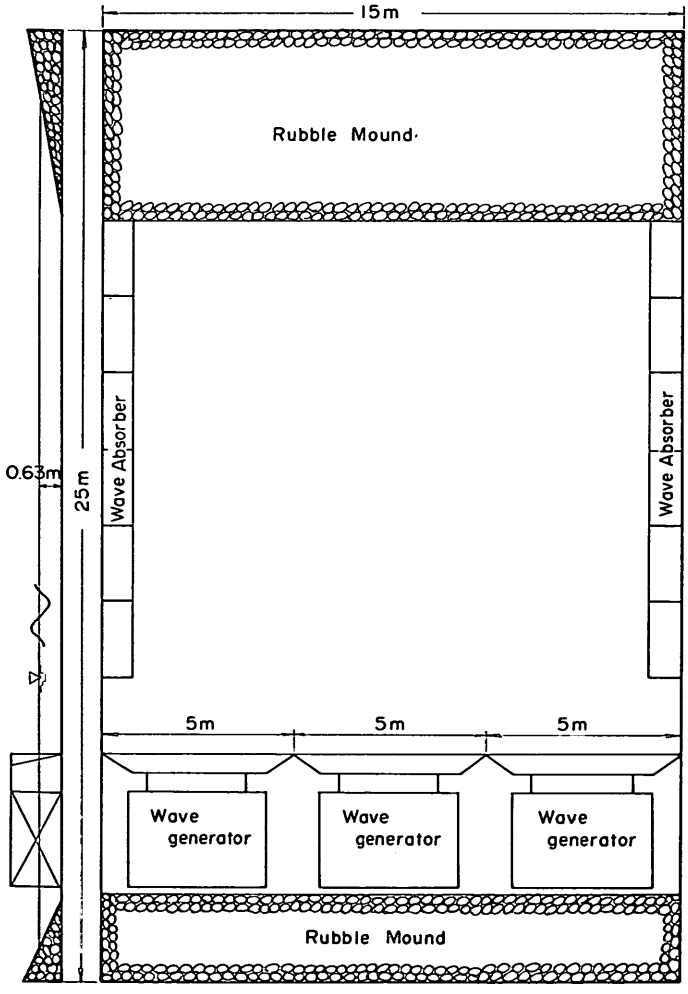

Fig. 14 Wave tank used in the experiments

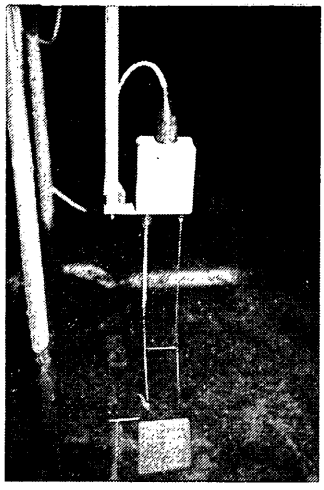

Photo. 1 Wave gauge

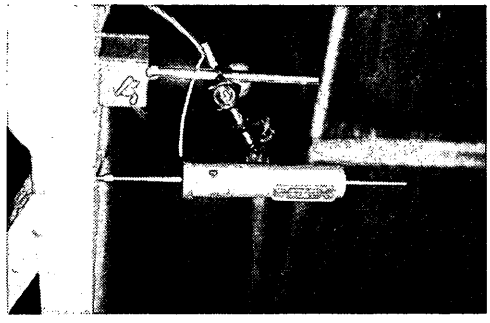

Photo. 2 Displacement gauge

and the others are kept at rest.

The waves produced by the single generator are measured by two wave gauges of capacitance type, shown in **Photo. 1**. The motion of the wave paddle is measured by a displacement gauge, which is fastened on the motionless adjacent paddle by magnet, as shown in **Photo. 2**. A pen recorder of 8 channels is used for recording wave profiles at two points and the motion of the wave paddle.

4.2 Experimental Conditions

Since the theoretical formula is derived under the assumption of small amplitude, the amplitude of the wave paddle motion must be held small, compared to the water depth and wave length. Therefore, the amplitude is determined to be kept about ± 2 cm. The wave paddle is moved periodically. The periods of the motion are 1 and 1.4 s.

The water depth is kept 0.63 m in the experiments. The wave lengths corresponding to 1 and 1.4 s become 1.54 and 2.73 m, respectively. The relative widths of b/L of the wave paddle are 3.2 and 1.83 for wave periods of 1 and 1.4 s, respectively.

The waves are measured at about 140 points in the front area, as shown in **Fig. 15**. The points except on the center line of the

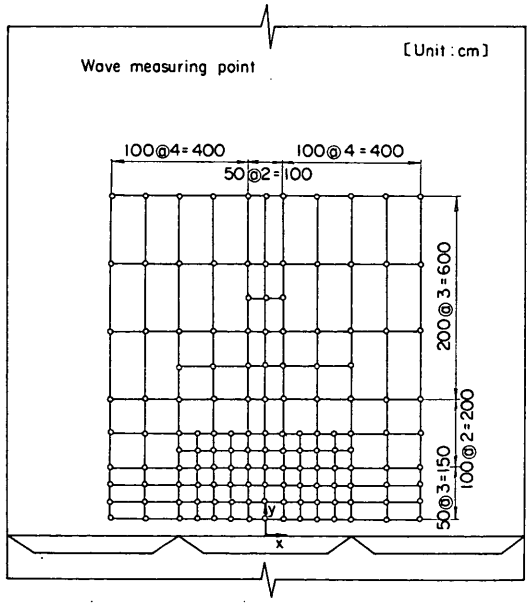

Fig. 15 Alignment of the wave measuring points

paddle are symmetrical to the center line. According to the theory, the wave heights at two points symmetrical to the line must have equal value each other. Then, average value at the two points symmetrical each other is taken as a wave height.

4.3 Comparison of Theoretical Values to Experimental Ones

Wave heights are computed as dimensionless value of $H/2Y_p$ in Eq. (56) which

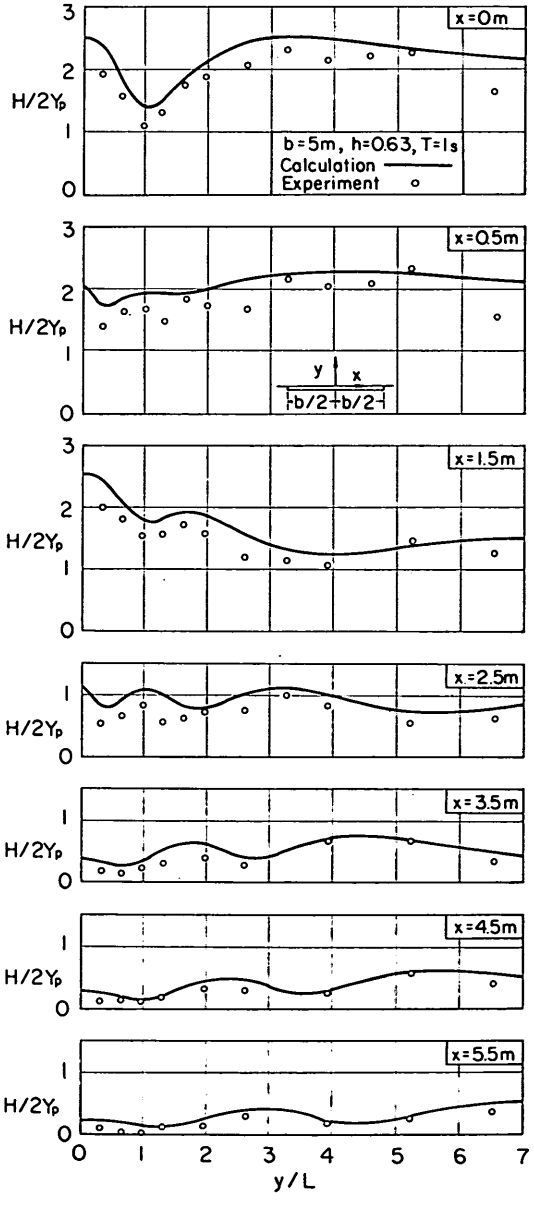

Fig. 16 Comparison of wave heights between computation and experiment on the lines pararallel to y-axis ($T=1.0$ s)

includes the stationary term, because the wave generator used in the experiments is of piston-type and wave height at the points of 0.5 m far from the wave paddle are affected by the stationary term. The comparison of the dimensionless wave heights $H/2Y_p$ between the computation and the experiment is shown in **Figs. 16** to **19**. The experimental value is expressed as an average at two point symmetrical to y-axis. **Figs. 16** and **17** are for the period of 1.0 s. On the other hand, **Figs. 18** and **19** are for the period of 1.4 s.

Figure 16 shows the comparison on the lines parallel to y-axis. The computed variations of $H/2Y_p$ to x/L draw wavy curves. On the line of x of 0 m which is a center line of the paddle, the computed value decreases down to 1.4 at y/L of 1 from 2.5 at 0 and begins to increase from the value. Then, it reaches maximum of 2.5 at y/L of 3.5, and gradually goes down as y/L becomes larger. The experimental values follow

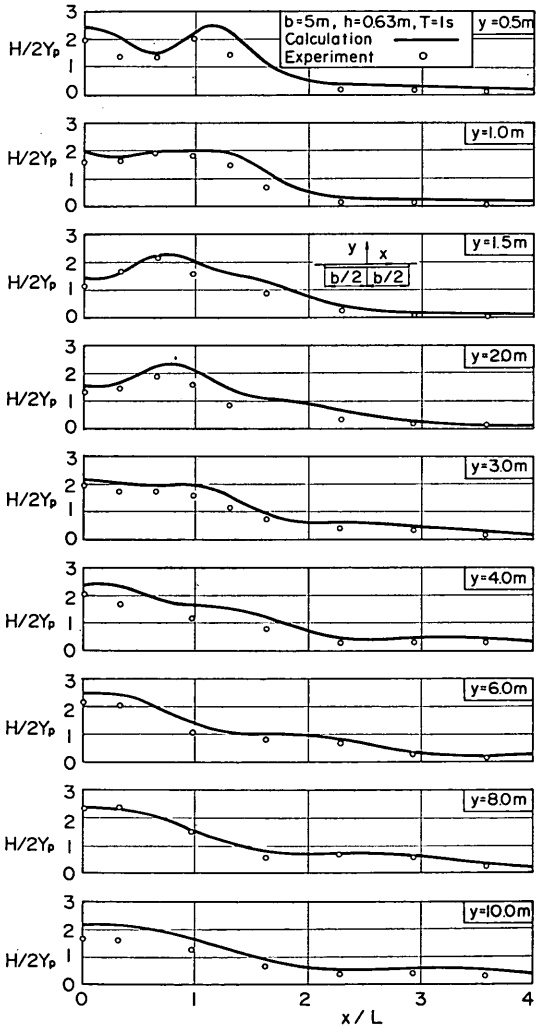

Fig. 17 Comparison of wave heights between computation and experiment on the lines parallel to x-axis ($T=1.0$ s)

the above variation quite well. However, they are plotted under the computed curve. The difference is about 0.2 in the value of $H/2Y_p$. The variations of the computed curves show quite different patterns for different lines of x. However, the experimental values show good agreement with the computed ones in the variational pattern, though they are a little bit smaller than the computed values.

In **Fig. 17**, where the comparison of $H/2Y_p$ between the computation and the experiment are made on the lines parallel to x-axis, the experimental values are a little smaller in the comparison to the computed ones, but their variations show good agreement with the patterns of the computed curves.

Figure 18 shows the comparison of $H/2Y_p$ for the period of 1.4 s on the lines parallel to y-axis. The wavy feature of the computed curves becomes weak in comparison to that of **Fig. 16**, because b/L decreases to 1.83 due to a long period. In the computed value on the wave paddle where $y/L=0$ and $x/L<2.5$, $H/2Y_p$ shows the value larger

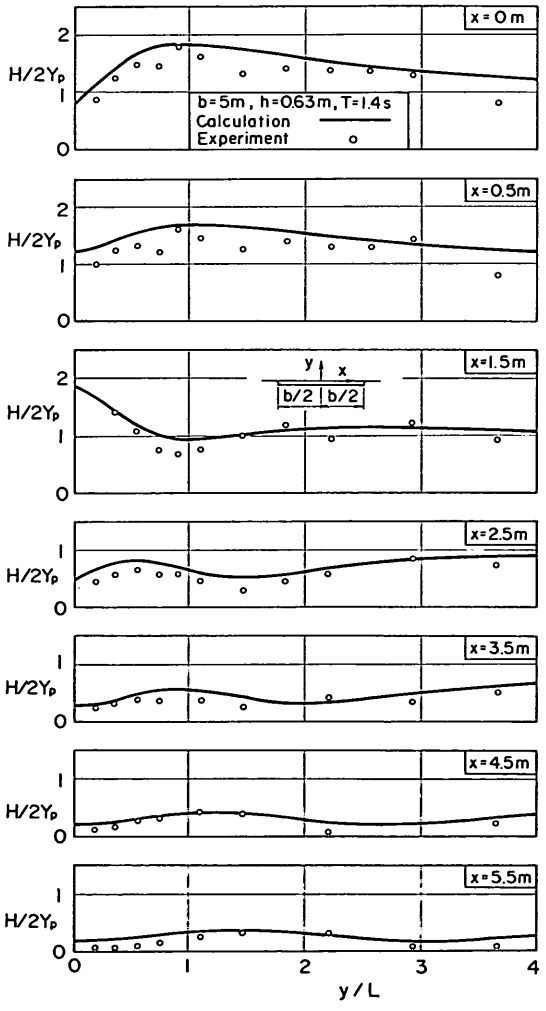

Fig. 18 Comparison of wave heights between computation and experiment on the lines parallel to y-axis ($T=1.4$ s)

than 2.0 in **Fig. 16**, but it becomes smaller than 2.0 in **Fig. 18**. On the line of x of 0 m the computed curve of $H/2Y_p$ goes up from 1.7 at y/L of 0, and after it reaches maximum of 1.8 at y/L of 0.8, it gradually goes down as y/L becomes larger. The experimental values quite well follow the above typical pattern, though they are plotted a little

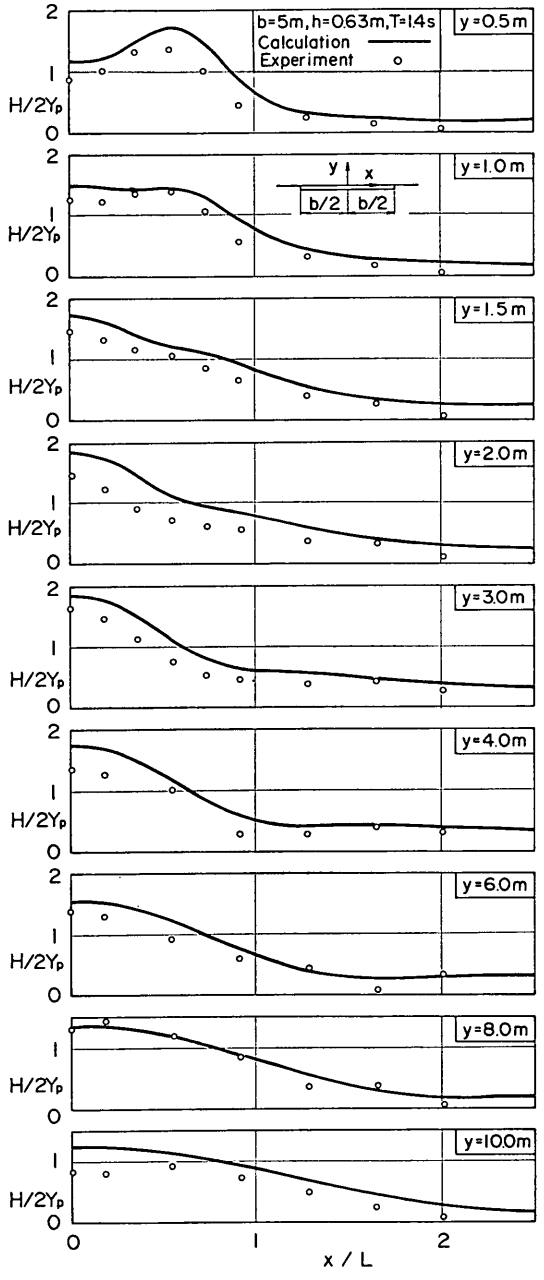

Fig. 19 Comparison of wave heights between computation and experiment on the lines parallel to x-axis ($T=1.4$ s)

under the computed curve. On the other lines of x, the experimental values are kept a little smaller than the computed ones, but their variations show good agreement with those of the computed curves.

Figure 19 shows the comparison on the lines parallel to x-axis. On the line of y of 0.5 m, variation of $H/2Y_p$ shows typical feature that the value of $H/2Y_p$ is small near the central line of y/L of 0, and highest at y/L of 0.6. In the portion of y/L larger than 0.6, the computed value goes down gradually. On the other lines, the values of $H/2Y_p$ indicate maximum at y/L of 0, and decline gradually as x/L becomes larger. The variation of experimental values follows that of the computed curve quite well, as mentioned above. However, the experimental values show the tendency that they are a little smaller than the computed ones.

In the comparison between the computation and the experiment shown in **Figs. 16** to **19**, the computed curve of $H/2Y_p$ shows good agreement with the variation of the experimental values, though the computed values themselve are a little larger than the experimental ones. Thus, the validity of the theoretical formula could be confirmed by the experiments.

As the causes of the difference between the computed value and the experimental one, the followings are picked up:

1) The wave paddle has not been built as it can slide on the tank floor. Therefore, the paddle has a clearance of about 4 cm between its lower end and the floor. Consequently, it happens that the wave energy leaks through the clearance, and that the waves are not generated by the paddle height equal to the water depth. By considering the clearance in wave generation[12], wave heights are reduced to 97% and 95% for the periods of 1.0 and 2.4 s, respectively.

2) The motion of the wave paddle creates aberration to the adjacent paddles. The aberration may disturb the waves and make them loss their energy.

It could not be estimated precisely how much the above causes affect wave height.

5. Theoretical Properties of Oblique Waves Generated by Serpent-type Wavemakers

5.1 Theoretical Formula of Oblique Waves

The velocity potential of waves generated by a single wave maker is expressed by Eq. (50). The velocity potential of oblique waves generated by a number of unit wavemakers can be obtained by linearly superposing Eq. (50). However, a phase difference between the motions of adjacent wavemakers must be considered in the superposition.

It is assumed that oblique waves can be generated successfully by a number of unit wave paddles of finite width b, as shown in **Fig. 10**. The wave has same phase on a line parallel to a crest line. Therefore, the following equation for the wave phase must be satisfied at two points on the line:

$$\frac{2\pi}{L}y-\sigma t=\frac{2\pi}{L_v}\left(y-\frac{b}{\tan\theta}\right)-(\sigma t+\epsilon) \quad , \tag{65}$$

where b denotes a distance in x-axis between two points of i and $(i+1)$ and corresponds to the width of a unit wave paddle, and L_v and θ are a wavelength in the direction

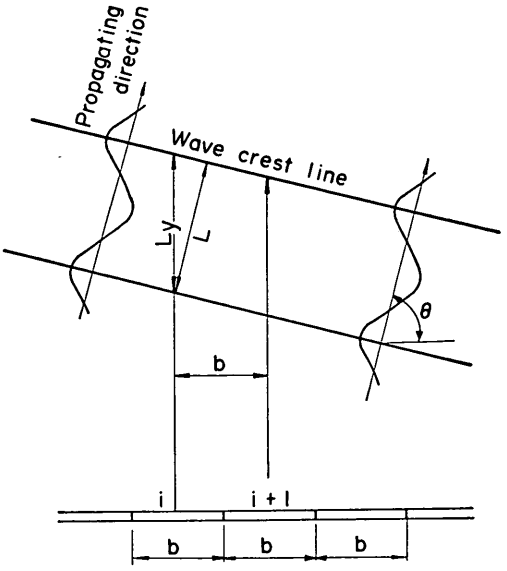

Fig. 20 Phase difference between the motions of adjacent wave paddles

of y-axis and a target angle of the propagation of the oblique waves, respectively. ϵ is a phase difference of the wave on line $(i+1)$ to that on line i.

Since L_y is given by

$$L_y = L/\sin\theta \ , \tag{66}$$

ϵ is obtained as

$$\epsilon = -\frac{2\pi}{L} b\cos\theta = -kb\cos\theta \ . \tag{67}$$

By using the phase difference ϵ given by Eq. (67) between the motions of the adjacent wave paddles, the velocity potential Φ_{0b} of the oblique wave is expressed in the following formula:

$$\begin{aligned}\Phi_{0b} = \sum_{i=-N_-}^{N_+} \Bigg[& \Bigg\{ \frac{\sigma}{k}(\alpha_p Y_p + \alpha_f Y_f) \frac{\cosh k(h+z)}{\sinh kh} \int_{-kb/2}^{kb/2} N_0\left(\sqrt{(kx-ikb-q)^2+(ky)^2}\right) dq \\ & - \sum_{\nu} \frac{\sigma}{\nu}(\beta_p Y_p + \beta_f Y_f) \frac{\cos \nu(h+z)}{\sin \nu h} \int_{-\nu b/2}^{\nu b/2} \frac{2}{\pi} K_0\left(\sqrt{(\nu x - i\nu b - q)^2 + (\nu y)^2}\right) dq \Bigg\} \\ & \times \cos(\sigma t - ikb\cos\theta) \\ & - \frac{\sigma}{k}(\alpha_p Y_p + \alpha_f Y_f) \frac{\cosh k(h+z)}{\sinh kh} \int_{-kb/2}^{kb/2} J_0\left(\sqrt{(kx-ikb-q)^2+(ky)^2}\right) dq \\ & \times \sin(\sigma t - ikb\cos\theta) \Bigg] \ ,\end{aligned} \tag{68}$$

where N_+ and N_- denote the numbers of wave paddles in possitive portion and negative one of x-axis, respectively, as shown in **Fig. 21**. Then, total number of the paddles is $(N_+ + N_- + 1)$. Equation (68) can be rewritten in the following form:

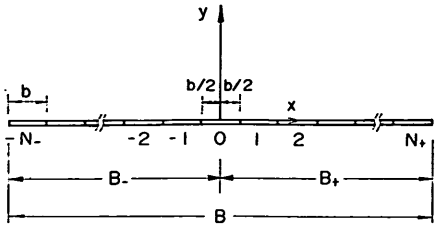

Fig. 21 Alignment of wave makers

$$\Phi_{0b}=\sum_{i=-N_-}^{N_+}\left[\left\{\frac{\sigma}{k}(\alpha_p Y_p+\alpha_f Y_f)\frac{\cosh k(h+z)}{\sinh kh}\int_{(i-1/2)kb}^{(i+1/2)kb}N_0(\sqrt{(kx-q)^2+(ky)^2})\,dq\right.\right.$$
$$\left.-\sum_{\nu}\frac{\sigma}{\nu}(\beta_p Y_p+\beta_f Y_f)\frac{\cos\nu(h+z)}{\sin\nu h}\int_{(i-1/2)kb}^{(i+1/2)kb}\frac{2}{\pi}K_0(\sqrt{(\nu x-q)^2+(\nu y)^2})\,dq\right\}$$
$$\times\cos(\sigma t-ikb\cos\theta)$$
$$-\frac{\sigma}{k}(\alpha_p Y_p+\alpha_f Y_f)\frac{\cosh k(h+z)}{\sinh kh}\left\{\int_{(i-1/2)kb}^{(i+1/2)kb}J_0(\sqrt{(kx-q)^2+(ky)^2})\,dq\right\}$$
$$\left.\times\sin(\sigma t-ikb\cos\theta)\right]\ . \tag{69}$$

By applying the Bernoulli equation (51) and by ignoring the stationary wave term, the dimensionless wave height R_H is given as follows:

$$R_H=\frac{H}{2(\alpha_p Y_p+\alpha_f Y_f)}$$
$$=\left[\left\{\sum_{i=-N_-}^{N_+}\left(\cos(ikb\cos\theta)\int_{(i-1/2)kb}^{(i+1/2)kb}N_0(\sqrt{(kx-q)^2+(ky)^2})\,dq\right.\right.\right.$$
$$\left.+\sin(ikb\cos\theta)\int_{(i-1/2)kb}^{(i+1/2)kb}J_0(\sqrt{(kx-q)^2+(ky)^2})\,dq\right)\Bigg\}^2$$
$$+\left\{\sum_{i=-N_-}^{N_+}\left(\cos(ikb\cos\theta)\int_{(i-1/2)kb}^{(i+1/2)kb}J_0(\sqrt{(kx-q)^2+(ky)^2})\,dq\right.\right.$$
$$\left.\left.\left.-\sin(ikb\cos\theta)\int_{(i-1/2)kb}^{(i+1/2)kb}N_0(\sqrt{(kx-q)^2+(ky)^2})\,dq\right)\right\}^2\right]^{1/2}\ . \tag{70}$$

The wave propagating angle γ of the oblique wave is determined in same manner as previously mentioned in **3.2**.

Judging from the distributions of wave height and direction shown in **Figs. 16** to **19**, the oblique waves can be expected to become more uniform as b/L becomes smaller. As b/L becomes infinitesimal, the summational form of Eq. (69) can be transformed to an integral form as follows:

$$\Phi_{0b}=\frac{\sigma}{k}(\alpha_p Y_p+\alpha_f Y_f)\frac{\cosh k(h+z)}{\sinh kh}\int_{-kB_-}^{kB_+}\left\{N_0(\sqrt{(kx-q)^2+(ky)^2})\right.$$
$$\times\cos(\sigma t-q\cos\theta)$$
$$\left.-J_0(\sqrt{(kx-q)^2+(ky)^2})\sin(\sigma t-q\cos\theta)\right\}dq\ , \tag{71}$$

where B_- and B_+ are equal to $(N_-+1/2)b$ and $(N_++1/2)b$, respectively, and the stationary wave term is ignored in Eq. (71). By applying the Bernoulli equation to Eq. (71), ths dimensionless wave height R_H defined by Eq. (70) can be obtained as follows:

$$R_H=\Bigg[\Bigg\{\int_{-kB_-}^{kB_+}[N_0(\sqrt{(kx-q)^2+(ky)^2})\cos(q\cos\theta)+J_0(\sqrt{(kx-q)^2+(ky)^2})\sin(q\cos\theta)]\,dq\Bigg\}^2+\Bigg\{\int_{-kB_-}^{kB_+}[J_0(\sqrt{(kx-q)^2+(ky)^2})\cos(q\cos\theta)-N_0(\sqrt{(kx-q)^2+(ky)^2})\sin(q\cos\theta)]\,dq\Bigg\}^2\Bigg]^{1/2}. \tag{72}$$

The wave propagating angle γ of the oblique wave for the infinitesimal width can be also determined by using the fluid velocity in the manner same as mentioned in **3.2**.

5.2 Characteristics of Wave Height and Propagating Angle

Wave profiles and propagating directions on the lines in a target direction have been computed under the conditions that total width $B=20$ m, a single paddle width $b=0.5$ m, a water depth $h=1$ m and a period T of the paddle motion$=1$ s. The results computed for piston-type wavemakers are shown in **Figs. 22** and **23**. **Figures 22** (a) and (b), respectively, show the wave profiles and the wave propagating direction for the target wave angle θ of 80°. As shown in **Fig. 22** (a), the distance between

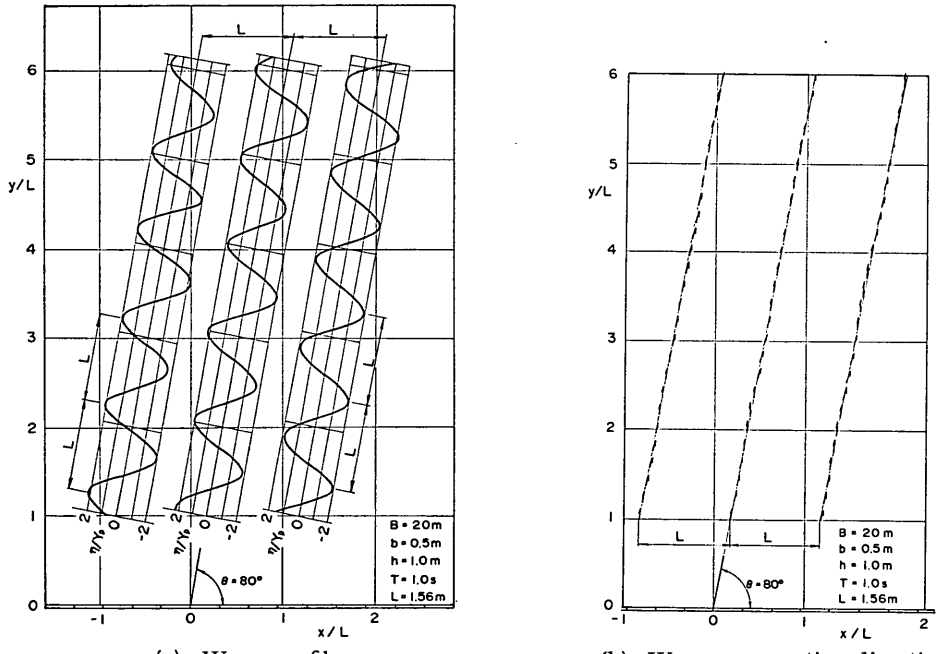

(a) Wave profile (b) Wave propagating direction

Fig. 22 Wave profile and propagating direction of the oblique wave propagating on the line of the target angle θ of 80°

successive wave crests coincides with the wave length L calculated by Eq. (8), but the elevations of wave crests or wave troughs are not uniform and depend on their locations.

Figure 22 (b) shows the wave propagating direction at each point on the lines. The direction is represented by short arrows. The wave direction differes a little at each point. The wave propagates as if a snake crawled. Consequently, the wave direction does not completely agree with the target one, and varies around the target direction. However, the wave propagates in the target direction on the average.

Figures 23 (a) and (b), respectively, show wave profiles and directions for the target angle of 60°. The distance between successive wave crests coincides with the wave length, which satisfies the dispersion relation of Eq. (8). The elevations of wave crests or wave troughs are not uniform and depend on their locations. The tendency of the non-uniformity in **Fig. 23** (a) is same as that in **Fig. 22** (a).

The wave direction shown in **Fig. 23** (b) does not coincide with the target wave direction, though the mean direction agrees with the target direction. The waves also propagate as if a snake crawled, as described above about **Fig. 22** (b).

By the above discussion of **Figs. 22** and **23**, it is clarified that the values of the wave height and propagating direction are not uniform, and depend on the location. Moreover, it is also clarified that on the average the wave propagates in the target direction of θ. In order to investigate the properties of the wave height and propagating angle in detail, they are computed for the target angles of 90°, 80°, 60° and 45° on the line parallel to x-axis. B and b in conditions of computation are same as those in **Figs. 22** and **23**, but they are represented in the dimensionless forms in the figures.

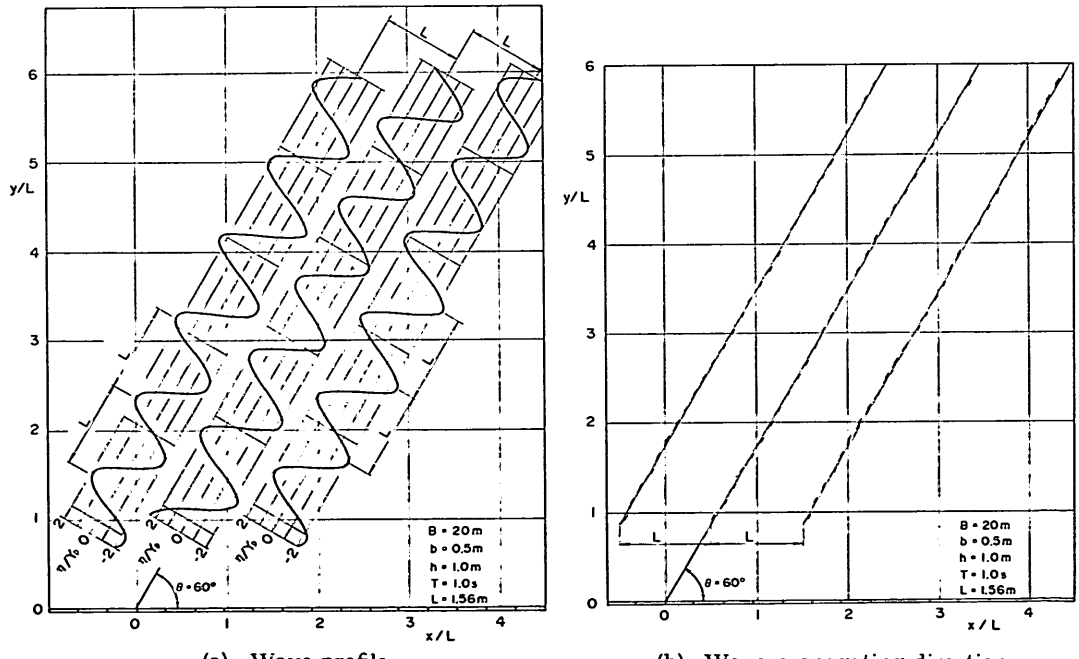

(a) Wave profile (b) Wave propagating direction

Fig. 23 Wave profile and propagating direction of the oblique wave propagating on the line of the target angle θ of 60°

In **Fig. 24** (a) for wave direction, on the line of y/L of 4, the wave propagating angle varies at a position, but the average angle is almost equal to the target angle of θ. In θ of 60°, γ approaches to 60°, showing wavy variation, and in x/L more than -3, the average of γ agrees with 60°. In θ of 45°, γ gradually approaches to 45°, showing wavy variation, and in x/L more than 1, the average of γ becomes 45°. The shift of the point where the mean value of γ agrees with a target angle θ depends on the value of θ. As θ becomes smaller, the point moves toward right side in the figure. Peak-to-peak distance of the wavy variation becomes shorter as θ is smaller. For example, the peak-to-peak distance relative to L is about 1.3 for 90° and 0.6 for 45°. In the cases that θ=60° and 45°, undulation pattern appears clearly in the variation of γ besides ripple pattern.

The variations of wave height and propagating angle on the line of y/L of 4 are shown in **Fig. 24** (b) where the computation is performed under the conditions same as those in **Fig. 24** (a). The wave height in the figure is represented by the dimensionless value of R_H defined by Eq. (70). The wave height shows wavy pattern even in the portion where the mean wave angle becomes almost uniform in **Fig. 24** (a). The wavy pattern consists of undulations and ripples. The undulating variation becomes more distinguishable as θ changes from 90° to 45°. In the portion of uniform mean value of γ, the value of R_H varies from 1.7 to 2.3 for 90°, from 1.7 to 2.4 for 80°, from 1.9 to 2.6 for 60° and from 2.0 to 3.1 for 45°. Thus, the variation of R_H grows greater in the portion, as θ becomes smaller.

Figures 25 (a) and (b) show the variations of wave angle γ and wave height R_H on the line of 8 in y/L, respectively. The line is twice as distant from the paddle as that in **Fig. 24**. In θ of 60° and 45°, the wave angle γ slowly approaches to the target angle of θ, and the portion of the mean uniform angle shifts more rightward in **Fig. 25** (a) than in **Fig. 24** (a). The wave propagating angle draws wavy pattern and the peak-to-peak distance in the wavy pattern decreases as θ becomes smaller. The variations of the wave height in **Fig. 25** (b) also show wavy patterns. The wavy pattern consists of undulations and ripples. The undulating variation is predominant and the ripple one is secondary, as θ is small like 60° and 45°.

The followings are drawn by the above discussion on the variations of the wave angle and wave height shown in **Figs. 24** and **25**:

1) Both wave angle and height show wavy feature and their values are not uniform

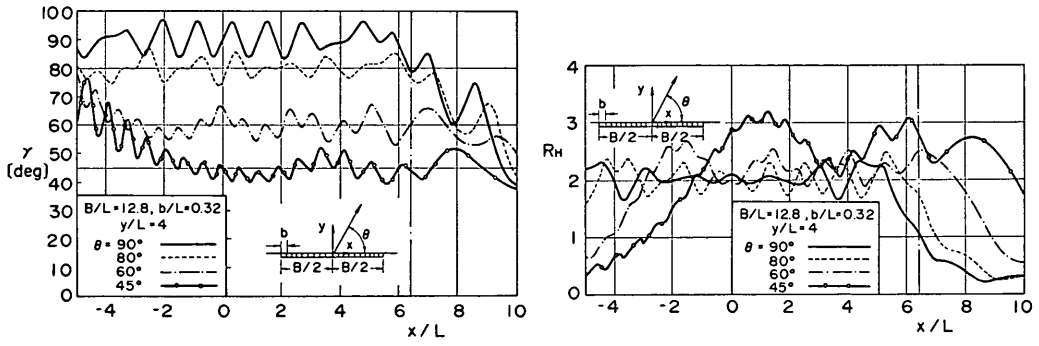

(a) Wave propagating direction (b) Wave height

Fig. 24 Variations of dimensionless wave height R_H and wave propagating angle γ to the target angle θ for y/L of 4

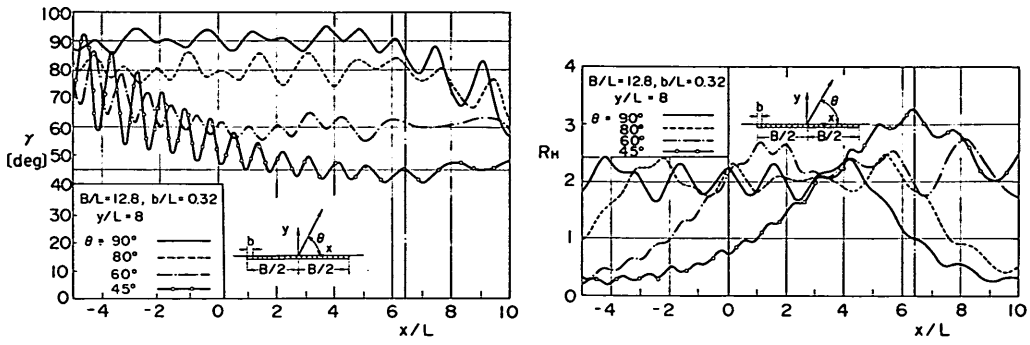

(a) Wave propagating direction (b) Wave height

Fig. 25 Variation of dimensionless wave height R_H and wave propagating angle γ to the target angle θ for y/L of 8

on the line of computation. The wave propagating angle γ agrees with the target angle θ on the average.

2) The wavy pattern of wave angle and height consist of the undulations and the ripples. The undulating variation is predominant and the ripple one is secondary, as the target angle θ is small like 60° and 45°.

5.3 Variations of Wave Height and Propergating Angle against Relative Width of a Unit Wave Paddle

It is clarified in the previous section of **5.2** that it is difficult to generate uniform oblique waves, even if the phase of the motions between the adjacent wave paddles is controlled. The variations of the wave propagating angle and the wave height depend on the relative width b/L of the paddle. Then, the dependency of their variations against the relative width is investigated numerically.

Figure 26 shows the theoretical variations of the wave propagating angle γ and the dimensionless wave height R_H for θ of 80° against various widths of b. The condition of the calculation is shown in the figure. The condition that b=0 m means that the width of the paddle is infinitesimal. The wave angle γ and the dimensionless wave height R_H show wavy features without regard to the value of b, but the features become weaker as the width b is smaller. In the figure, the variations of γ and R_H are much small different between 0 m and 1 m of b. For b of 2 m, however, γ and R_H vary from 60° to 90° and from 1 to 2.7, respectively. Thus, the variations are very large, compared to the variations in b of 0 m or 1 m.

In **Fig. 27** for θ of 60°, the value of γ for b other than 2.0 m varies around the target angle of 60°, but for 2.0 m varies from 90° to 145°. In the case that b=2.0 m, the value of R_H varies between 0.5 and 2.7. Thus, the variation of R_H is very large for b of 2 m. The width of 2.0 m is quite useless for the period of 1.0 s to generate uniform oblique waves. It is better to let b smaller in order to make the wave propagating angle γ closer to the target angle of 60°. In the wave height, R_H varies more slowly as b becomes smaller, but the variation shows little difference among the values of b less than or equal to 1 m, though the variation becomes more undulating in the smaller value of b. Our interest is attracted in the theoretical fact that the mean value of R_H becomes larger in the portion of γ close to the target angle, as the value of b is smaller.

In **Fig. 28** for θ of 45°, the width b of 2.0 m is found inadequate in generation of

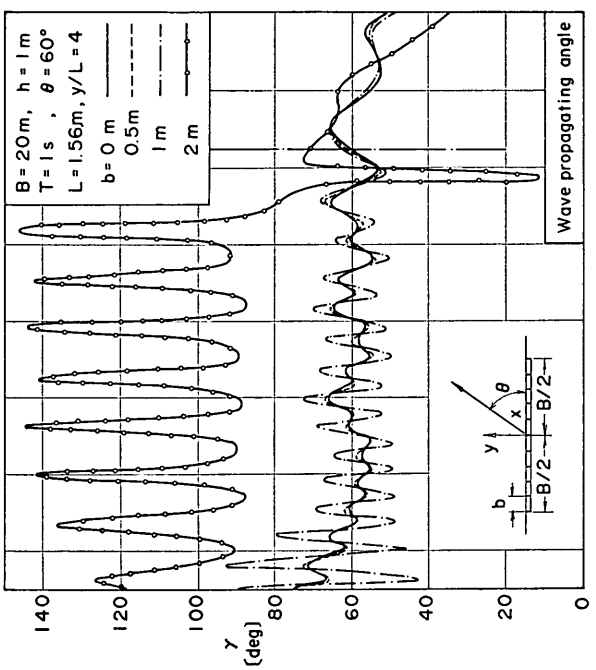

Fig. 27 Variation of wave propagating angle and wave height for various values of b ($\theta=60°$)

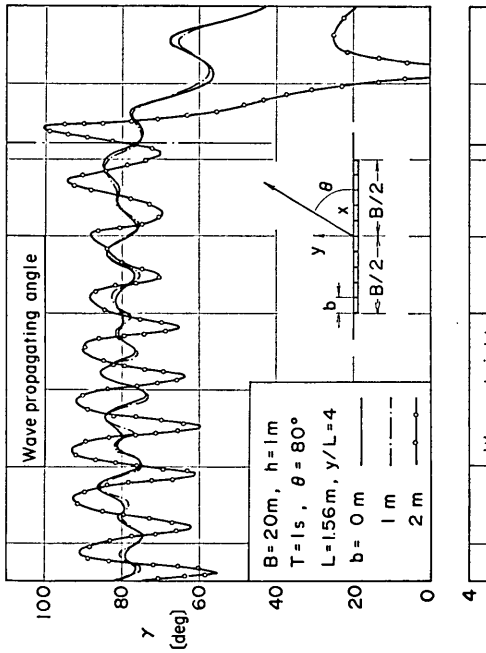

Fig. 26 Variation of wave propagating angle and wave height for various values of b ($\theta=80°$)

oblique waves, because the value of γ is far from the target angle of 45°. Even in b of 1 m, a great difference from θ of 45° appears in the portion of x/L less than 0. For x/L more than 0, however, the wave angle γ shows the tendency of gradual convergence to the target angle of 45°, oscillating around the line of 45°. The amplitude of the oscillation is large, compared to that of 0 m, or 0.5 m. The difference of between the widths of 0 m and 0.5 m is negligibly small. The variation of γ becomes smaller as b approaches to small value, but even if b is made infinitesimal, the wavy pattern cannot be made to disappear. On the other hand, the wave height shows variational feature of undulation as b becomes smaller. The curve for b of 1 m shows largest variation with short peak-to-peak distance. The undulating variation appears more distinguish-

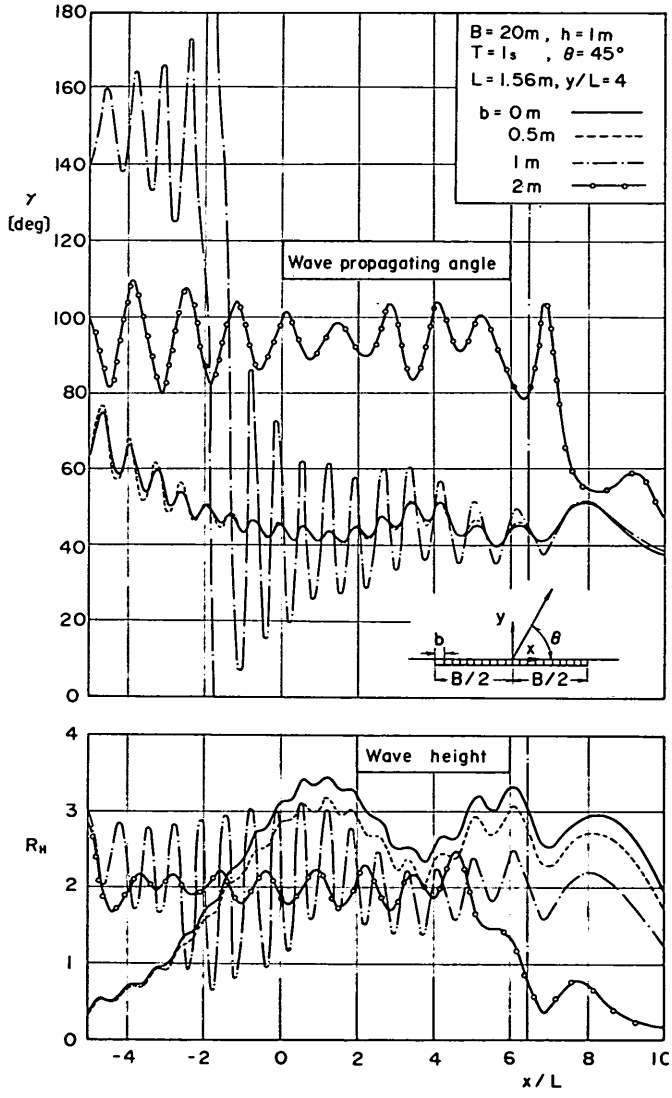

Fig. 28 Variations of wave propagating angle and wave height for various values of b (θ=45°)

able, as b approaches to a small value. In b of 0 m, the value of R_H varies slowly from 2.3 to 3.3.

The above discussion on **Figs. 26** to **28** draws the following conclusions:

1) In order to make the wave propagating angle uniform and close to the target angle, it is necessary to let the width of the paddle shorter as the target angle becomes smaller.
2) The variations of γ and R_H always show wavy features regardless of the value of b. Even if the width of b is made infinitesimal, it is impossible to remove their wavy patterns. The variation of γ, however, become smaller, as b becomes more shortened.
3) The undulating variation of R_H grows more distinguishable, as b becomes smaller.

5.4 Oblique Waves in a Wave Tank with Reflective Side Walls

In the previous section, the oblique waves in a wave tank of infinite width and length or in no reflection tank from side walls are discussed. In an ordinary wave tank, waves are reflected from the side walls.

In this section, the waves in a tank with reflective side walls are theoretically investigated by using mirror image method. It is assumed that both side walls reflect the waves completely. In the mirror image method, an infinite number of wave tanks symmetrical to the basin walls are imaged in both sides of the tank, as shown in **Fig. 29**, and in each imaginary tank, oblique waves are generated in the direction symmetrical each other to the walls. The waves in the real tank can be expressed as the superposition of these imaginary waves. This is formulated as follows:

$$\Phi_{re}=\Phi_{0b}+\sum(\Phi_L+\Phi_R) \ , \tag{73}$$

where Φ_{re} and Φ_{0b} denote the velocity potentials in the real tank with the walls and in the imaging tank without the walls, respectively, and Φ_L and Φ_R are the velocity potentials of the imaginary tank without the walls in the left side and the right one, respectively. By using Eq. (69), Eq. (73) can be rewritten as follows:

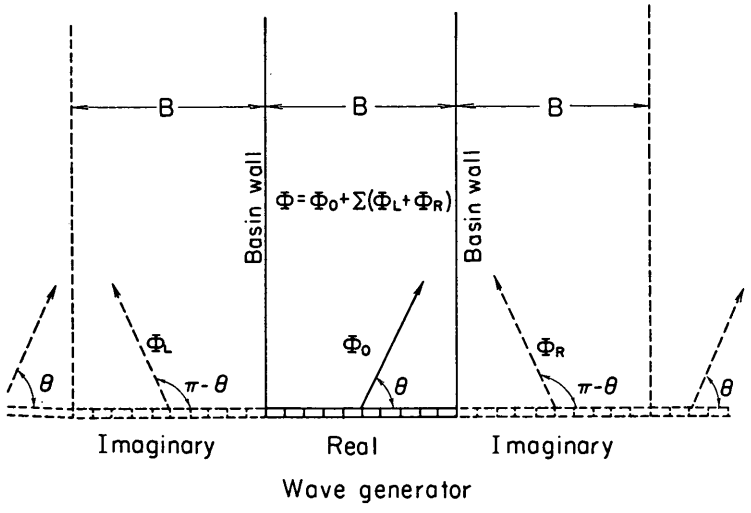

Fig. 29 Schematic figure of mirror image method for estimating waves in a wave tank

$$\Phi_{rs} = \sum_{j=-\infty}^{\infty} \sum_{i=-N}^{N} \frac{\sigma}{k}(\alpha_p Y_p + \alpha_f Y_f)\frac{\cosh k(h+z)}{\sinh kh}$$
$$\times \int_{(i-1/2)kb+jkB}^{(i+1/2)kb+jkB} \{N_0(\sqrt{(kx-q)^2+(ky)^2}) \cos[\sigma t-(-1)^j kb\cos\theta]$$
$$-J_0(\sqrt{(kx-q)^2+(ky)^2}) \sin[\sigma t-(-1)^j kb\cos\theta]\}\, dq\ , \qquad (74)$$

where the stationary wave term are ignored and the origin of the coordinates (x, y) is placed at the center of the tank width. When b is infinitesimal, Eq. (71) is used instead of Eq. (69). The computation is carried out on the three lines parallel to the wave paddles. The distances of the lines from the wave paddles are shown in **Fig. 30**. The waves on the line of 8 m nearest to the paddles will not be much influenced by the reflected waves, and on the middle line of 17 m, the influence of the reflected waves is supposed to reach the central part of the line. On the most distant line of 34 m, the reflected waves will give influence in a whole width. The influential portion of the reflected waves is determined in the optical reflection.

According to the mirror image method, an infinite number of imaginary wave tanks must be considered, but in the computation, a wave tank is imagined in each side to save computing time. **Figures 31** to **33** show the variations of γ and R_H on the nearest line, the middle one and the most distant one, respectively. In each figure, a dash-circle line represents the variations of γ and R_H without the side walls.

On the nearest line of **Fig. 31**, typical standing waves appear in the vicinity of the right side wall, where the wave propagating angle γ shows a feature of radical change. The peaks of R_H appear in every wave length L distant, which coincides with the distance calculated. In comparison between the curves for b of 0 m and 1 m, the dash line of 1 m varies slowly, while the solid one of 0 m does finely. In the value of R_H the solid line wholly gives larger value than the dash one. In the central part of the tank, the wave propagating angle of solid line and dash one are close to the target angle of 60° on the average, though they show ripple features.

In **Fig. 32**, the line of computation is 17 m distant from the paddles. The influential portion of reflected waves by the optical reflection is in right side from the center of the tank, but the influence of the reflected waves spreads over the whole width, judging from the variation of the wave height in **Fig. 32** computed by the theo-

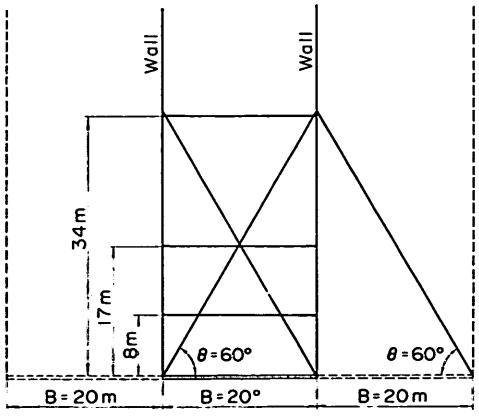

Fig. 30 Alignment of computing lines and optical reflection from side wall

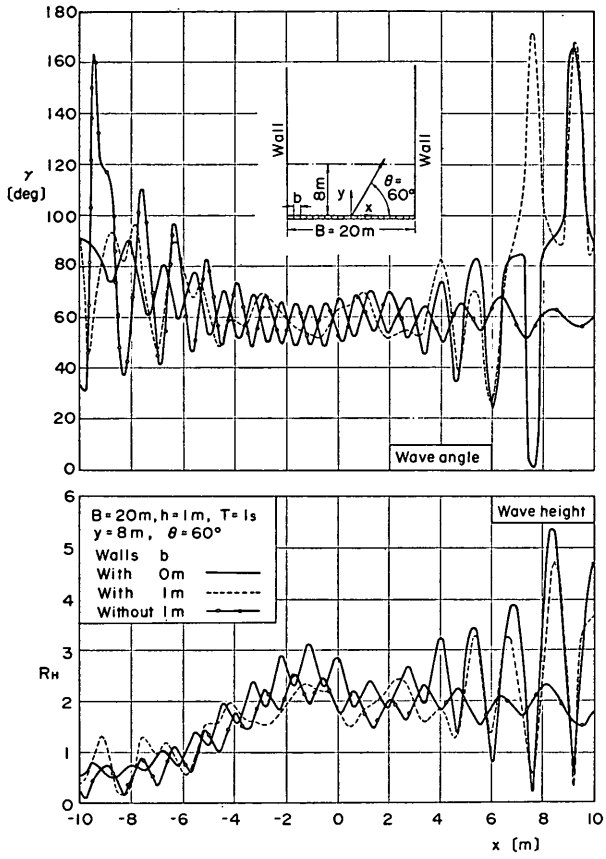

Fig. 31 Variations of propagating angle and wave height on the line of y of 8 m

retical formula. The degree of the influence decreases towards the left side wall. It is found that the distinguished standing waves appear in the portion of x/L more than -3 and the peaks of their heights appear in every wave length L of 1.56 m. On the line there is no portion of almost uniform angle of the wave propagation.

On the line of 34 m, the appearance of the reflected waves only is estimated by the optical reflection. The wave propagating angle γ varies small around 120° except the neighborhood of the right side wall as shown in **Fig. 33**. Consequently, it is clarified that the waves on the line propagate in the reflective direction and that they are reflected waves from the right side wall. The dimensionless wave height R_H shows a wavy feature and varies between 2 and 3. On this line, additional one pair of imaginary tanks seems to be necessary in order to estimate the wave height and propagating angle more precisely.

As mentioned in the above discussion of **Figs. 31** to **33**, in a wave tank with the reflective side walls, the standing waves are produced by the reflection from side walls, and the wave height and propagating angle vary largely. It is impossible to generate oblique waves uniform in height and propagating angle, even if the separation of incident waves and reflected is done.

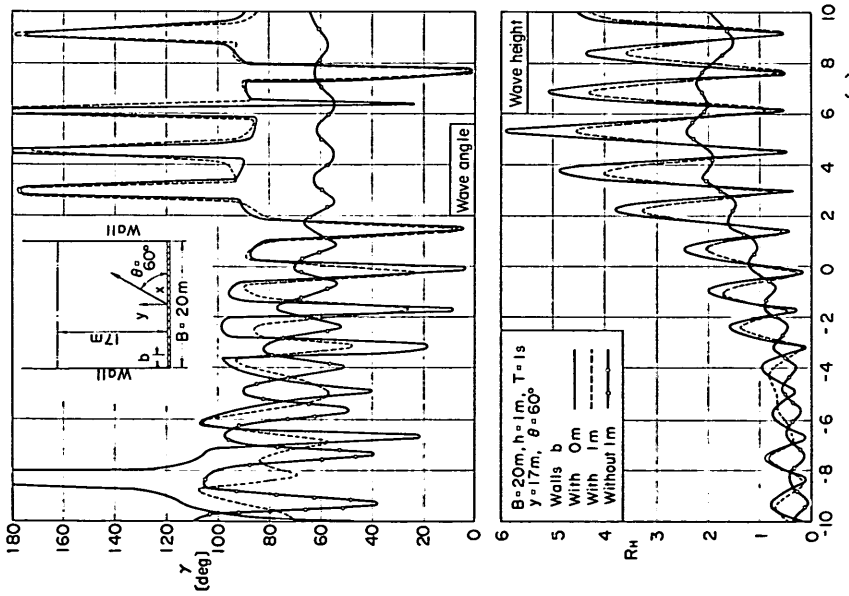

Fig. 32 Variations of propagating angle and wave height on the line of y of 17 m

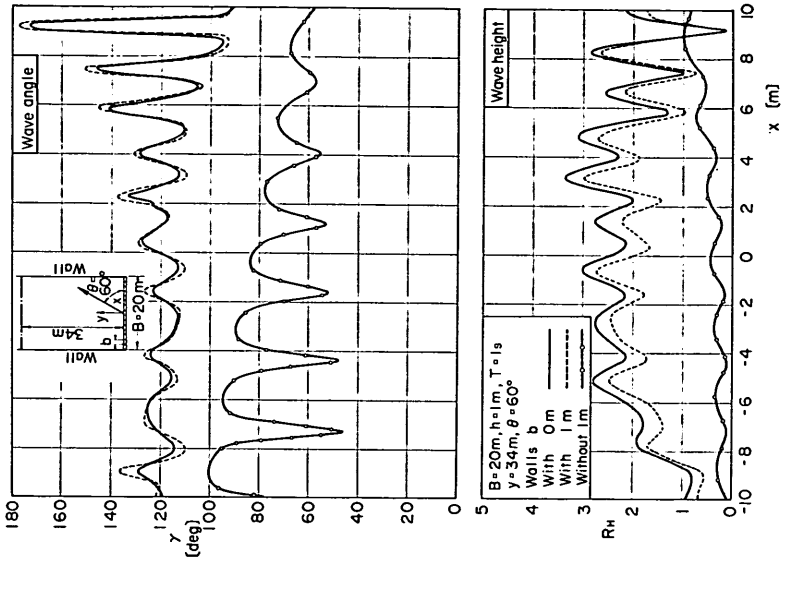

Fig. 33 Variations of propagating angle and wave height on the line of y of 34 m

6. Discussions

6.1 Problems of a Temporarily Used Wave Channel Built in a Wave Basin

As mentioned in the previous chapter of **3**, it has been clarified that waves generated by a single wavemaker show the wavy feature and the snakelike propagation on the line parallel to the paddle, even if the width of the wave paddle is fairly wide. We often build a temporary wave channel inside a wave basin, as shown in **Fig. 34**. All wave paddles in the basin are not operated, but one or few paddles among them in front of the channel are operated for saving energy. If the tips of the side walls of the channel are distant from the paddles, the wavy feature and the snakelike propagation of the generated waves are unavoidable in front of the paddles. When the waves with the feature enter the channel, they propagate in it, being reflected from the side walls. In the consequence, the wave height in the channel does not become uniform widthwide, but the variation of the wave height appears. To prevent the non-uniformity of the wave height, the tips of the wall should be made to approach to the wave paddle as far as possible.

Figure 35[18] shows the variation of wave height in front of two wave paddle, each of which is 5 m wide. The wave heights were measured for estimation of the height of incident wave which passes through the opening between the breakwaters, whose alignment is represented by dash lines in the figure. The waves used in the experiments are unidirectional irregular waves and the distribution of the wave height is drawn as the ratio to the mean significant wave height in the measured area with uniform depth. The wave height varies at point to point. The variation seems to be caused by the wavy feature described above. At the time of the experiments, we had no consideration of the wavy feature caused by the finite width of the paddle, but we expected that waves had uniform height in the central narrow area without receiving the influence the end of the paddles. When we make experiments in the alignment of the wave paddles like the above, we must take care of the appearance of the wavy feature and elaborate to prevent it.

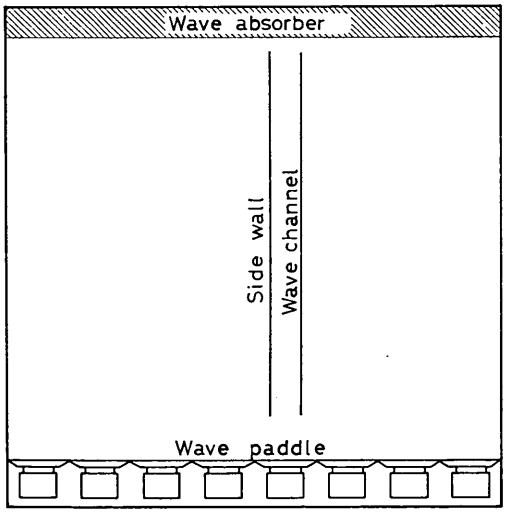

Fig. 34 Temporary wave channel built inside the wave basin

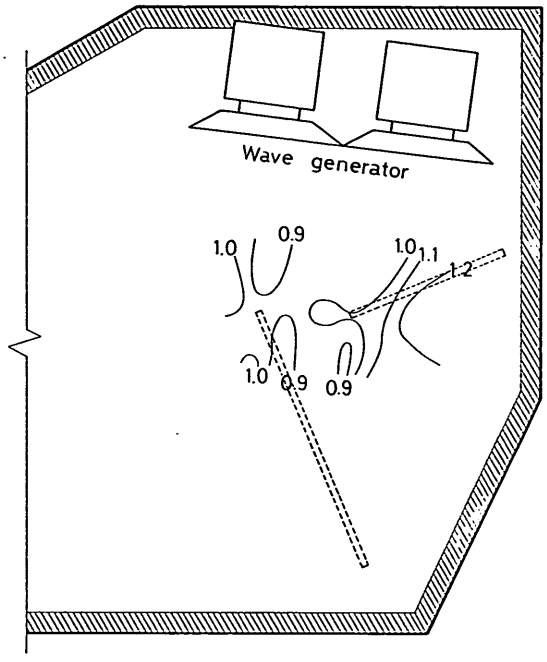

Fig. 35 Distribution of irregular wave height in front of wave paddles

6.2 Generation of Directional Random Waves

It has seemed the best way to use oblique waves as component wave in the uniform generation of the directional random waves. In the theoretical analysis of the oblique waves, it is clarified that the oblique waves generated by serpent-type wavemakers do not show uniform heights and propagating directions, but vary, depending on their locations. In especial, the variation of the wave heights become larger, as the target angle of the wave propagation becomes smaller.

Consequently, it cannot be expected that uniform directional random waves are produced by the generation of the oblique wave as a component one. We must allow the variation of the directional spectrum as far as serpent-type wavemakers are used. The detail discussion on the variation of directional spectrum will be carried on in a future paper.

7. Conclusions

The following conclusions can be drawn from the present study on the oblique waves generated by serpent-type wavemakers:

1) The velocity potential of waves generated by a single wavemaker is theoretically derived under the assumption of small motion in the wave paddle, as given by Eq. (50).
2) In the result of the computation of wave height, the stationary wave term included in Eq. (50) is neglegible except the vicinity of the wave paddle.
3) For the ratio of paddle width to wavelength or b/L smaller than 0.5, the contour

lines of the height and the propagating angle of the waves generated by a single wavemaker show the concentric feature and radiative one, respectively. They cross orthogonally each other. However, the contour lines of the wave height become of more complex pattern and cross slantly to those of the wave angle, as the value of b/L become larger.

4) Even if b/L is as large as 12.8, the wave height shows wavy feature, and varies from point to point. The variation becomes gradually smaller as the value of b/L becomes larger, but it remains even for b/L of 64.
5) The theoretical values of wave heights agree well with the experimental ones. Consequently, the theoretical formula has been confirmed to be valid for the estimation of wave height.
6) The theoretical formula for oblique waves is obtained as the superposition of the velocity potential in Eq. (50) by considering the phase difference of the motions between adjacent wave paddles.
7) The oblique waves generated by serpent-type wavemakers show wavy feature in their height and propagating angle, which depend on the value of b/L, target wave angle θ, and the location of interest.
8) The wavy variation of the height and propagating angle of oblique waves consist of ripple and undulation patterns. The undulation pattern becomes more predominant in the variation, as the target angle θ becomes smaller.
9) The wavy variation of the height and the propagating angle of the oblique waves is impossible to make disappear, even if the width of the unit wave paddle is made infinitesimal.
10) The oblique waves in a wave tank with reflective side walls are computed with the consideration of the reflected waves from the side walls. In the computed results, the standing waves appear in the vicinity of the wall on the line in parallel to and near the paddle, and the portion of the standing waves spreads more broadly as the line becomes more distant from the paddles. On the line sufficiently distant, the reflected waves only appear and they propagate in the direction of the reflection from the side wall. The height and propagating angle always show wavy features.

Acknowledgement

The author wishes to express his sincere gratitude to Dr. Yoshimi Goda, Director of Hydraulic Engineering Division, and Mr. Yasumasa Suzuki, Senior Researcher of Marine Hydrodynamics Division, for their useful suggestions and discussions during the development of the theoretical analysis.

A special dept of gratitude is owed to Mr. Shigehide Amano, a trainee from Penta Ocean Construction Co., Ltd., who assisted the author in performance of the experiments and the computations and drafted all figures appearing in this paper.

(Received on March 31, 1982)

References

1) MITSUYASU, H. et al.: Observation of the directional spectrum of ocean waves using a cloverleaf bouy, J. Geophys. Res., Vol. 5, No. 4, 1975, pp. 750~760.
2) COTE, L. J. et al.: The directional spectrum of a wind generated sea as determined from data obtained by the Stereo Wave Observation Project, Meteorological

Papers, Vol. 2, No. 6, New York Univ., 1960, 88 p.
3) GODA, Y. and Y. SUZUKI: Computation of refraction and diffraction of sea waves with Mitsuyasu's directional spectrum, Tech. Note of Port and Harbour Res. Inst., No. 230, 1975, 45 p. (*in Japanese*)
4) GODA, Y., T. TAKAYAMA, and Y. SUZUKI: Diffraction diagram for directional random waves, Proc. 16th Coastal Engg. Conf., 1978, pp. 628~650.
5) HUNTINGTON, S. M. and D. M. THOMPSON: Forces on a large vertical cylinder in multi-directional random waves, OTC 2539, 1976.
6) Edinburgh Wave Power Project, Fourth Year Report, Vol. 3 of 3, 1978
7) NAESER H.: Generation of uniform directional spectra in a wave basin using the natural diffraction of waves, POAC79, 1979, pp. 621~632.
8) ZIEKIEWICZ, O. C., P. BETTESS, and D. W. KELLY: The finite element method for determing fluid loading on rigid structures two- and three-dimensional formulations, Numerical Method in Offshore Engineering edited by O. C. Zienkiewicz, R. W. Lewis and K. G. Stagg, Wiley, 1978, pp. 141~183.
9) CHURCHILL, R. V.: Operational Mathematics, third eddition, McGraw-Hill, 481 p.
10) CAMPBELL, G. A. and R. M. FOSTER: Fourier Integrals for Practical Applications, D. Van Nostrand Co., INC., 1967, 177 p.
11) Biésel, F., F. Suquet and others: Les apparails générateurs de hoale en laboratoire, La Houille Blanche, Vol. 6, Nos. 2, 4, et 5, 1951 (*translated by St. Anthony Falls, Hyd. Lab., Univ. Minnesota, Rept. No. 39*).
12) Madsen, O. S.: Waves generated by a piston-type wavemaker, Proc. 12th Coastal Engg. Conf., 1970, pp. 589~607.
13) TAKAYAMA, T. and Y. KAMIYAMA: Diffraction of sea waves by rigid or cusuion type breakwaters, Rept. Port and Harbour Res. Inst., Vol. 16 No. 3, 1977, pp. 3~37.

List of Symbols

A^c : an unknown coefficient of $\bar{\phi}_k^c$ in Eq. (30)
A^s : an unknown coefficient of $\bar{\phi}_k^s$ in Eq. (30)
B : total width of wave paddles
B_+ : total width in possitive x
B_- : total width in negative x
B^c : an unknown coefficient of $\bar{\phi}_k^c$ in Eq. (30)
B^s : an unknown coefficient of $\bar{\phi}_k^s$ in Eq. (30)
b : width of a wave paddle
C^c : an unknown coefficient of $\bar{\phi}_k^c$ in Eq. (30)
C^s : an unknown coefficient of $\bar{\phi}_k^s$ in Eq. (30)
D^c : an unknown coefficient of $\bar{\phi}_k^c$ in Eq. (30)
D^s : an unknown coefficient of $\bar{\phi}_k^s$ in Eq. (30)
$F(x)$: an odd function
$\tilde{F}(\lambda)$: cosine transform of $F(x)$
$G(x)$: an odd function
$\tilde{G}(\lambda)$: cosine transform of $G(x)$
g : acceleration of gravity
H : wave height
h : water depth
$J_0(x)$: Bessel function with index zero
$J_1(x)$: Bessel function with index one
$K_0(x)$: modified Bessel function with index zero
k : wave number, $k=2\pi/L$
L : wavelength
L_y : $L_y=L/\sin\theta$

N_+ : number of wave paddle in possitive x
N_- : number of wave paddle in negative x
$N_0(x)$: Neumann function with index zero
$N_1(x)$: Neumaan function with index one
R_H : dimensionless wave height
r : distance from the origin, $r=\sqrt{x^2+y^2}$
T : period of the paddle motion
t : time
u : fluid velocity in x-direction
$(u)_{max}$: component of V_{max} in x-direction
V : $V=\sqrt{u^2+v^2}$
V_{max} : maximum of V
v : fluid velocity in y-direction
$(v)_{max}$: component of V_{max} in y-direction
x : horizontal axis parallel to the wave paddle
Y_p : amplitude of y_p
Y_f : amplitude of y_f
y : horizontal axis normal to the wave paddle
y_0 : displacement of the wave paddle at the still water surface
y_p : parallel displacement of the paddle
y_f : rotational displacement of the paddle at the still water surface
z : vertical axis, possitive upwards
α_p : $\alpha_p=\sinh^2 kh \Big/ \left\{kh\left[1+\dfrac{\sinh 2kh}{2kh}\right]\right\}$
α_f : $\alpha_f=\sinh kh\,[\sinh kh-(\cosh kh-1)/kh] \Big/ \left\{kh\left[1+\dfrac{\sinh 2kh}{2kh}\right]\right\}$
β_p : $\beta_p=\sin^2 \nu h \Big/ \left\{\nu h\left[1+\dfrac{\sin 2\nu h}{2\nu h}\right]\right\}$
β_f : $\beta_f=\sin \nu h\,[\sin \nu h+(\cos \nu h-1)/\nu h] \Big/ \left\{\nu h\left[1+\dfrac{\sin 2\nu h}{2\nu h}\right]\right\}$
γ : wave propagating angle
γ_p : $\gamma_p=\arctan(y/x)$
ϵ : phase difference between adjacent wave paddles
η : displacement of water surface
θ : target wave angle
λ : a parameter in cosine transformation
ν : real solution of Eq. (9)
σ : angular frequency of the paddle motion, $\sigma=2\pi/T$
Φ : velocity potencial of waves generated by a single wavemaker
Φ_{0b} : velocity potential of oblique waves
Φ_{re} : velocity potential of oblique waves in a tank with reflective side walls
$\phi^c(x,y)$: a function concerned to $\cos \sigma t$
$\phi^s(x,y)$: a function concerned to $\sin \sigma t$
$\phi_k^c(x,y)$: an unknown function concerned to $\cos \sigma t$ and $\cosh k(h+z)$
$\bar{\phi}_k^c$: cosine transform of ϕ_k^c
$\phi_k^s(x,y)$: an unknown function concerned to $\sin \sigma t$ and $\cosh k(h+z)$
$\bar{\phi}_k^s$: cosine transform of ϕ_k^s
$\phi_\nu^c(x,y)$: an unknown function concerned to $\cos \sigma t$ and $\cos \nu(h+z)$
$\bar{\phi}_\nu^c$: cosine transform of ϕ_ν^c
ϕ_ν^s : an unknown function concerned to $\sin \sigma t$ and $\cos \nu(h+z)$
$\bar{\phi}_\nu^s$: cosine transform of ϕ_ν^s